Neoclassical transport in strong gradient regions of large aspect ratio tokamaks

Silvia Trinczek [1]†, Felix I. Parra [1], Peter J. Catto [2], Iván Calvo [3] and Matt Landreman [4]

[1]Princeton Plasma Physics Laboratory, Princeton, NJ 08543, USA

[2]Plasma Science and Fusion Center, Massachusetts Institute of Technology, Cambridge, MA, USA

[3]Laboratorio Nacional de Fusión, CIEMAT, Madrid, 28040, Spain

[4]University of Maryland, College Park, MD 20742, USA

(Received xx; revised xx; accepted xx)

We present a new neoclassical transport model for large aspect ratio tokamaks where the gradient scale lengths are of the size of the poloidal gyroradius. Previous work on neoclassical transport across transport barriers assumed large density and potential gradients but a small temperature gradient, or neglected the gradient of the mean parallel flow. Using large aspect ratio and low collisionality expansions, we relax these restrictive assumptions. We define a new set of variables based on conserved quantities, which simplifies the drift kinetic equation whilst keeping strong gradients, and derive equations describing the transport of particles, parallel momentum and energy by ions in the banana regime. The poloidally varying parts of density and electric potential are included. Studying contributions from both passing and trapped particles, we show that the resulting transport is dominated by trapped particles. We find that a non-zero neoclassical particle flux requires parallel momentum input which could be provided through interaction with turbulence or impurities. We derive upper and lower bounds for the energy flux across a transport barrier in both temperature and density and present example profiles and fluxes.

1. Introduction

The pedestal, and transport barriers in general, play an important role in tokamak performance (Wagner *et al.* 1984; Greenfield *et al.* 1997) and thus it is useful to find a comprehensive transport model for these regions. In pedestals, for example, strong gradients of temperature, density and radial electric field of the order of the inverse poloidal gyroradius are observed (Viezzer *et al.* 2013). Moreover, it has been found that the ion energy transport in pedestals is close to the neoclassical level (Viezzer *et al.* 2018). Measurements of H-mode pedestals in Alcator C-Mod (Theiler *et al.* 2014; Churchill *et al.* 2015) and Asdex-Upgrade (Cruz-Zabala *et al.* 2022) have shown poloidal variations of density, electric field and ion temperature that cannot be explained using standard neoclassical theory. It is thus desirable to extend neoclassical theory for stronger gradients, and logical to choose the ion poloidal gyroradius as the characteristic scale length. Comparisons of experimental data with standard neoclassical theory (Hinton & Hazeltine 1976) such as the one by Viezzer *et al.* (2018) miss finite poloidal gyroradius effects.

Setting the scale length in transport barriers to be the poloidal gyroradius implies

† Email address for correspondence: strincze@pppl.gov

that the poloidal component of the $E \times B$-drift in large aspect ratio tokamaks becomes of the order of the poloidal component of the parallel velocity. As a result, a strong radial electric field shifts the trapped-passing boundary (Shaing *et al.* 1994*a*), and causes an exponential decrease proportional to the radial electric field in plasma viscosity (Shaing *et al.* 1994*a*) and radial heat flux (Kagan & Catto 2010; Shaing & Hsu 2012). The mean parallel flow is also affected by a strong radial electric field and can change direction (Kagan & Catto 2010). A strong shear in radial electric field causes orbit squeezing, which reduces the heat flux and increases the trapped particle fraction for increasing radial electric field shear (Shaing & Hazeltine 1992; Shaing *et al.* 1994*b*).

Combining all these effects, Shaing & Hsu (2012) calculated the heat flux and mean parallel velocity but they neglected the strong mean parallel velocity gradient and the poloidal variation of the electric potential. Kagan & Catto (2008) and Catto *et al.* (2013) have likewise developed extensions to neoclassical theory to allow for stronger density gradients to calculate fluxes. In (Kagan & Catto 2010; Catto *et al.* 2011, 2013), the density gradient was taken to be steep but the temperature gradient scale length had to be much larger than the ion orbit width. Furthermore, they assumed a quadratic electric potential profile and also neglected the poloidal variation of the potential.

Comparisons between analytical solutions and simulations have been carried out by Landreman *et al.* (2014), which demonstrated the significance of source terms.

We will assume that the gradient length scale of potential, density and temperature is of the order of the poloidal gyroradius and we will retain the poloidal variations of density and potential. Assuming a large aspect ratio tokamak with circular flux surfaces in the banana regime and including unspecified sources of particles, parallel momentum and energy, we find equations for the ion distribution function, and a set of transport relations for ions.

In section 2, we justify our choice of orderings physically, and we motivate our choice of sources of particles, momentum and energy by considering the transition from the core into a transport barrier. A more detailed discussion of trapped and passing particles follows in section 3, where the shift of the trapped-passing boundary is derived and a new set of variables based on conserved quantities is introduced. In section 4 we calculate the ion distribution function in the trapped-barely-passing and freely passing regions. We also calculate the poloidally varying part of density and potential. The solvability conditions for the equation containing the distribution function of the bulk ions are the density, parallel momentum and energy conservation equations, calculated in section 5. The ion transport equations are discussed further in section 6. We find that a non-zero parallel momentum input is required to sustain a neoclassical particle flux and consider the possibility of interaction with turbulence. For the energy flux, we derive upper and lower bounds and relate the gradient lengths of temperature and density to the growth of neoclassical energy flux as one moves into the transport barrier. We conclude by presenting some example profiles for the "high flow" case and the "low flow" case. A summary of our results is given in section 7.

2. Orderings and phase space outline

In this paper we consider the transition from regions with large turbulent transport into strong gradient regions. In a region of large turbulent transport, for example the core, neoclassical transport gives a minor contribution because turbulent transport carries most particles, momentum and energy. With the transition into a regime of low turbulence, like a transport barrier, the same total fluxes must be kept but as turbulence decreases, we anticipate that the turbulent transport goes down, too, and instead the fluxes must

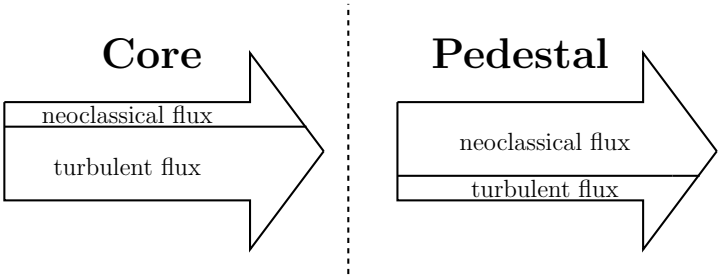

FIGURE 1. The total flux must be kept constant across the core and pedestal. The neoclassical contribution increases in the pedestal whereas the turbulent fluxes decrease as turbulence quenches. There is the possibility of interaction between turbulent and neoclassical transport in the pedestal.

be picked up by neoclassical transport. Thus, we expect a rise in neoclassical fluxes at the transition from core to, for example, a pedestal (see figure 1). This argument is consistent with the observation that the energy flux in the pedestal is close to its neoclassical value (Viezzer *et al.* 2018). We will see, however, that this simple picture of the top of a transport barrier has limitations. In section 6.1 we find constraints that prevent the neoclassical fluxes from growing with radius.

Turbulence and neoclassical transport could interact in the transport barrier and hence we need to include a source Σ in the neoclassical picture. This source represents any possible input from turbulence as well as external injection of particles, momentum and energy. The source must balance the neoclassical fluxes $\Sigma/f \sim n^{-1}|\nabla\psi|(\partial\Gamma/\partial\psi) \sim n^{-1}T^{-1}|\nabla\psi|(\partial Q/\partial\psi)$, where Γ is the neoclassical particle flux, Q is the neoclassical energy flux, n is the density, T is the ion temperature, and ψ is the poloidal flux divided by 2π, which we use as a flux surface label. To estimate the size of Σ, we need the size of the neoclassical particle and energy fluxes. We consider trapped and passing particles separately.

We can estimate the contributions from trapped and passing particles to particle and energy transport by making random walk estimates. The diffusion coefficient D for a random walk is $D \sim (\Delta x)^2/\Delta t$, with Δx and Δt the random walk size and time, respectively. The neoclassical particle flux is thus

$$\Gamma \sim \frac{(\Delta x)^2}{\Delta t}\frac{n}{L_n}, \tag{2.1}$$

where $L_n = |\nabla \ln n|^{-1}$. In a large aspect ratio tokamak, where $r/R \sim \epsilon \ll 1$, r is the minor radius and R is the major radius, the poloidal gyroradius is much bigger than the gyroradius. For passing particles we will show that the orbit widths are $\Delta x \sim \epsilon\rho_p$, where $\rho_p = qR\rho/r$ is the poloidal gyroradius, q is the safety factor and ρ is the gyroradius. The time between collisions is $\Delta t \sim 1/\nu$, where ν is the collision frequency. The gradient of density is assumed to be of the order of the poloidal gyroradius and so the particle flux due to passing particles is

$$\Gamma_p \sim (\epsilon\rho_p)^2\nu\frac{n}{\rho_p} \sim \epsilon q\nu n\rho. \tag{2.2}$$

The orbit width for trapped particles will turn out to be $\Delta x \sim \sqrt{\epsilon}\rho_p$, the collisional time is $\Delta t \sim \epsilon/\nu$ and again the density gradient length is $L_n \sim \rho_p$. The fraction of trapped particles in phase space is only $\sim \sqrt{\epsilon}$, and with that we arrive at a neoclassical particle

flux due to trapped particles of order

$$\Gamma_t \sim \sqrt{\epsilon}(\sqrt{\epsilon}\rho_p)^2 \frac{\nu}{\epsilon}\frac{n}{\rho_p} \sim \frac{q}{\sqrt{\epsilon}}\nu n \rho. \tag{2.3}$$

A comparison of the transport contribution from passing and trapped particles shows that the particle flux due to trapped particles is much larger,

$$\frac{\Gamma_p}{\Gamma_t} \sim \epsilon^{3/2} \ll 1. \tag{2.4}$$

The same estimate can be performed for the neoclassical energy flux when substituting the energy gradient nT/L_T for the particle density gradient n/L_n, where $L_T \sim L_n \sim \rho_p$. In section 5 we find transport equations that are consistent with this estimate and show that transport is dominated by trapped particles.

Using the sizes of particle and energy flux above, we can now give an estimate for the source Σ that we have to introduce in the kinetic equation to mimic turbulence, particle, momentum and energy sources. The gradient of the particle flux is

$$|\boldsymbol{\nabla}\psi|\frac{\partial \Gamma}{\partial \psi} \sim \frac{\Gamma_t}{\rho_p} \sim \sqrt{\epsilon} n \nu \tag{2.5}$$

and hence we include a source

$$\Sigma \sim \sqrt{\epsilon}\nu f. \tag{2.6}$$

3. Fixed-θ variables

To calculate the particle orbits, we introduce a new set of variables: the fixed-θ variables, which are based on the conserved quantities energy $\mathcal{E}$, canonical angular momentum ψ_*, and magnetic moment μ,

$$\mathcal{E} = \frac{1}{2}v^2 + \frac{Ze\Phi}{m}, \qquad \psi_* = \psi - \frac{I v_\parallel}{\Omega}, \qquad \mu = \frac{v_\perp^2}{2B}. \tag{3.1}$$

Here, v is the ion velocity, m is the ion mass, Ze is the charge, ψ is the flux function, Ω is the Larmor frequency, and B is the magnetic field strength. The electric potential is $\Phi = \phi + \phi_\theta$, where ϕ and ϕ_θ denote the components which give the radial and poloidal electric field, respectively. The piece ϕ only has radial dependence, $\phi = \phi(\psi)$, and its size is given by $e\phi/T \sim 1$, whereas ϕ_θ is the small poloidally varying part of the electric potential, so $\phi_\theta = \phi_\theta(\psi, \theta)$ and $e\phi_\theta/T \sim \epsilon$. Here, θ is the poloidal angle. Throughout this work we will use that the electric potential is of the form

$$\phi_\theta = \phi_c \cos\theta, \tag{3.2}$$

which we will prove to be true in the banana regime for circular flux surfaces in section 4.4. Energy, canonical angular momentum and magnetic moment are constant in time, so following the trajectory of a single particle, we find

$$\frac{1}{2}v_\parallel^2 + \mu B + \frac{Ze}{m}\Phi(\psi,\theta) = \frac{1}{2}v_{\parallel f}^2 + \mu B_f + \frac{Ze}{m}\Phi(\psi_f, \theta_f) \tag{3.3}$$

and

$$\psi - \frac{I v_\parallel}{\Omega} = \psi_f - \frac{I v_{\parallel f}}{\Omega_f}, \tag{3.4}$$

where the subscript f indicates the values of the respective quantities at a fixed poloidal angle θ_f, which represents a reference point in the orbit of the particle. It is important

to note that ψ_f and $v_{\|f}$ are constants for each particle. For example, following the trajectory of a passing particle, its velocity will deviate from $v_{\|f}$, but, having assumed the conservation laws above, the particle returns to its initial position ψ_f with the velocity $v_{\|f}$ after one complete poloidal turn. Another particle on a different orbit will have a different $v_{\|f}$ and ψ_f. Hence, the fixed-θ quantities can be understood as labels of orbits and will be used as new phase space variables later on. The angle θ_f is left as a choice at this point, because choosing $\theta_f = 0$ only captures particles that are trapped on the low-field side whereas setting $\theta_f = \pi$ captures particles trapped on the high-field side. We show in Appendix D.1 that it is important to take both sides into account when calculating trapped particle effects.

Using the standard large aspect ratio, circular flux surface tokamak, we can write the magnitude of the magnetic field as

$$B \simeq B_0 \left(1 - \frac{r}{R}\cos\theta\right) \tag{3.5}$$

to first order in the inverse aspect ratio ϵ. Here, B_0 is the magnetic field on the magnetic axis. For $\theta_f = 0$, the magnetic field is

$$B \simeq B_f \left[1 + \frac{r}{R}(1 - \cos\theta)\right], \tag{3.6}$$

with $B_f = B_0(1 - r/R)$, whereas for $\theta_f = \pi$ the magnetic field can be written as

$$B \simeq B_f \left[1 - \frac{r}{R}(1 + \cos\theta)\right] \tag{3.7}$$

with $B_f = B_0(1 + r/R)$. Changing θ_f from $\theta_f = 0$ to $\theta_f = \pi$ causes a jump in B_f of $O(\epsilon)$. It will be important in Appendix D that this difference is small.

In transport barriers, strong gradients in density, pressure and electric potential are observed. We will assume that $L_n \sim L_T \sim L_\Phi \sim \rho_p$. Ordering the characteristic length of the transport barrier to be of the order of the poloidal gyroradius implies that the poloidal component of the $E \times B$-drift is of the same order as the poloidal component of the parallel velocity. The poloidal component of the $E \times B$-drift is

$$\frac{c}{B}(\boldsymbol{E} \times \hat{\boldsymbol{b}}) \cdot \boldsymbol{\nabla}\theta = \frac{cI}{B}\frac{\partial \Phi}{\partial \psi}\hat{\boldsymbol{b}} \cdot \boldsymbol{\nabla}\theta \equiv u\hat{\boldsymbol{b}} \cdot \boldsymbol{\nabla}\theta + \frac{cI}{B}\frac{\partial \phi_\theta}{\partial \psi}\hat{\boldsymbol{b}} \cdot \boldsymbol{\nabla}\theta. \tag{3.8}$$

Here, $E = -\boldsymbol{\nabla}\Phi$ is the electric field, c is the speed of light, and $\hat{\boldsymbol{b}} = \boldsymbol{B}/B$, where the magnetic field is $\boldsymbol{B} = I\boldsymbol{\nabla}\zeta + \boldsymbol{\nabla}\zeta \times \boldsymbol{\nabla}\psi$ and ζ is the toroidal angle. We have defined the velocity

$$u = \frac{cI}{B}\frac{\partial \phi}{\partial \psi}. \tag{3.9}$$

Due to our choice of ordering, u and the parallel velocity $v_\|$ are of the same size. The poloidal velocity in this case is

$$\left(v_\|\hat{\boldsymbol{b}} + \frac{c}{B}\boldsymbol{E} \times \hat{\boldsymbol{b}}\right) \cdot \boldsymbol{\nabla}\theta \simeq \left(v_\| + u\right)\hat{\boldsymbol{b}} \cdot \boldsymbol{\nabla}\theta. \tag{3.10}$$

Particles are trapped on banana orbits if their poloidal velocity goes to zero at any point on their orbit. In the case of strong radial electric field this requires $v_\| + u = 0$ instead of the usual trapping condition $v_\| = 0$, as was first argued by Shaing *et al.* (1994*a*). It follows that particles with a parallel velocity close to $-u$, where u is not necessarily small, are trapped. It has been previously shown that in this case the width of the trapped-barely-passing region in velocity space is $\sim \sqrt{\epsilon}v_t$, where v_t is the thermal speed (Shaing & Hazeltine 1992). We re-derive this result by calculating the deviations in radial position

and velocity of particles on trapped orbits in Appendix A. Passing particles do not get reflected. One can divide the phase space into the freely passing region where $v_\parallel + u \sim v_t$ and the trapped-barely-passing region $v_\parallel + u \sim \sqrt{\epsilon} v_t$.

For freely passing particles, we show in Appendix A.1 that $v_\parallel - v_{\parallel f} \sim \epsilon v_t$ and $\psi - \psi_f \sim \epsilon \rho_p R B_p$, where B_p is the poloidal magnetic field. Thus, the deviations in parallel velocity and radial location are small in ϵ. The deviations become large and diverge when $v_\parallel + u$ becomes small. This is the trapped-barely-passing region. For trapped-barely-passing particles, the differences are still small but larger by $\sqrt{\epsilon}$, so $v_\parallel - v_{\parallel f} \sim \sqrt{\epsilon} v_t$ and $\psi - \psi_f \sim \sqrt{\epsilon} \rho_p R B_p$ as can be found in Appendix A.2.

From equation (A 13), which was first derived in this form by Shaing *et al.* (1994*a*) (see their equation (22)), we can deduce that particles are trapped for

$$\frac{(v_{\parallel f} + u_f)^2}{2} \leqslant \left\{ S_f \left[\left(\mu B_f - v_{\parallel f} u_f \right) \left(\frac{B}{B_f} - 1 \right) + \frac{Ze}{m} (\phi_\theta - \phi_{\theta f}) \right] \right\} \Big|_{\max} . \tag{3.11}$$

The quantity S is the squeezing factor as defined by Hazeltine (1989)

$$S = 1 + \frac{cI^2}{B\Omega} \frac{\partial^2 \phi}{\partial \psi^2} . \tag{3.12}$$

Equation (3.11) implies that $v_{\parallel f} + u_f \sim \sqrt{|S_f|\epsilon} v_t$, which is consistent with Shaing & Hazeltine (1992). In our case, $S_f \sim 1$ and $\epsilon \ll 1$ and hence $v_{\parallel f} \simeq -u_f$ holds, to lowest order, in the trapped-barely-passing region. We can rewrite (3.11) setting $v_{\parallel f} \simeq -u_f$

$$\frac{(v_{\parallel f} + u_f)^2}{2} \leqslant \left\{ S_f \left[\left(\mu B_f + u_f^2 \right) \left(\frac{B}{B_f} - 1 \right) + \frac{Ze}{m} (\phi_\theta - \phi_{\theta f}) \right] \right\} \Big|_{\max} . \tag{3.13}$$

Now we see that the term on the right hand side containing u_f^2 is the centrifugal force that pushes particles towards the outboard midplane and is small in low flow neoclassical theory. Here, both the magnetic mirror force and the centrifugal force can trap particles on the outboard side. For $\phi_c > 0$, the electric potential can oppose the magnetic mirror and the centrifugal force and if the electrostatic force is strong enough, it can cause trapping of particles on the inboard side. This will become relevant in Appendix D.

Example orbits for trapped and passing particles for a circular-flux-surface tokamak are shown in figure 2. In the figure, we emphasise the difference between the width of trapped and passing particle orbits.

4. Banana regime

The drift kinetic equation follows from an expansion of the Vlasov equation in ρ/L. In our case, this expansion is equivalent to an expansion in ϵ because $\rho/L \sim \rho/\rho_p \sim \epsilon$, where $\rho/R \sim \epsilon^2$. Keeping only terms of order $O(\epsilon^3 \Omega f)$, the steady state drift kinetic equation for an ion distribution function $f(\psi, \theta, v_\parallel, \mu)$ is

$$\begin{aligned} \left(v_\parallel \hat{\boldsymbol{b}} + \boldsymbol{v}_E \right) \cdot \boldsymbol{\nabla} \theta \frac{\partial f}{\partial \theta} + \left(\boldsymbol{v}_E + \boldsymbol{v}_M \right) \cdot \boldsymbol{\nabla} \psi \frac{\partial f}{\partial \psi} \\ + \left[\hat{\boldsymbol{b}} + \frac{v_\parallel}{\Omega} \hat{\boldsymbol{b}} \times \left(\hat{\boldsymbol{b}} \cdot \boldsymbol{\nabla} \hat{\boldsymbol{b}} \right) \right] \cdot \left(-\mu \boldsymbol{\nabla} B + \frac{Ze}{m} \boldsymbol{E} \right) \frac{\partial f}{\partial v_\parallel} = C[f, f] + \Sigma, \end{aligned} \tag{4.1}$$

where $\boldsymbol{v}_E$ is the $E \times B$-drift, $\boldsymbol{v}_M = \mu \hat{\boldsymbol{b}} \times \boldsymbol{\nabla} B / \Omega + v_\parallel^2 \hat{\boldsymbol{b}} \times (\hat{\boldsymbol{b}} \cdot \boldsymbol{\nabla} \hat{\boldsymbol{b}}) / \Omega$ is the magnetic drift, $C[f, f]$ is the Fokker-Planck ion-ion collision operator and we include a source $\Sigma \sim \sqrt{\epsilon} \nu f$, which is consistent with our estimate in section 2. Note that we are neglecting terms small

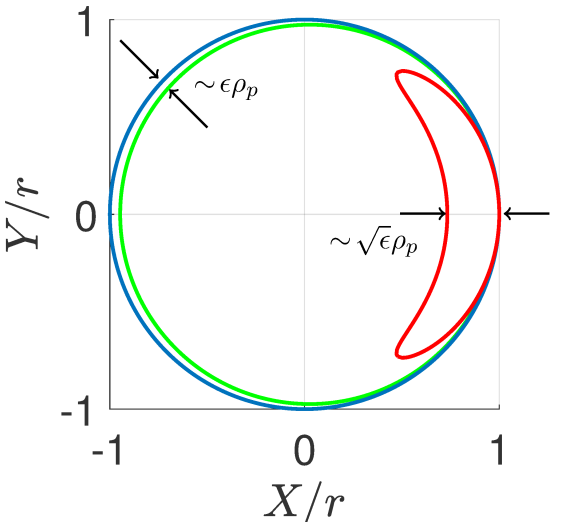

FIGURE 2. Orbits of passing (green) and trapped (red) particles which follow from (A 4) and (A 16) are shown for $r/R = 0.1$ and circular flux surfaces (blue). We chose $\theta_f = 0$, $\phi_\theta = 0$, $\mu B_f/v_t^2 = 1$, $\Omega_f\psi_f/(Iv_t) = 1$, $u_f/v_t = 1.5$ and $S_f = 1.5$. We use $v_{\|f}/v_t = -u_f/v_t + 5$ for the example passing particle trajectory and $v_{\|f}/v_t = -u/v_t + 0.2$ for the trapped particle trajectory. The spatial coordinates X and Y determine the position in the poloidal plane with respect to the magnetic axis. To make the orbits visible, we have chosen a flux surface with radius $r = \sqrt{X^2 + Y^2} = \Omega\psi_f/(Iv_t)$, but note that we assume $r \ll \Omega\psi_f/(Iv_t)$ in the rest of the paper. The deviation from the flux surface are much larger for trapped particles than for passing particles.

in ϵ. It is convenient to make a change of variables from $(v_\|, \psi)$ to the fixed-θ variables $(v_{\|f}, \psi_f)$. The resulting drift kinetic equation is

$$\dot{\theta}\frac{\partial f}{\partial \theta}\bigg|_{v_{\|f},\psi_f} = C[f,f] + \Sigma, \tag{4.2}$$

where $\dot{\theta} = (v_\|\hat{\boldsymbol{b}} + \boldsymbol{v}_E)\cdot\boldsymbol{\nabla}\theta$, $f = f(\psi_f, \theta, v_{\|f}, \mu)$ and the derivative in θ is holding $v_{\|f}$ and ψ_f fixed. To lowest order one can approximate $\dot{\theta} \simeq (v_\| + u)/qR \gtrsim \epsilon^{1/2}v_t/qR$. Imposing collisionality in the banana regime $qR\nu/(\epsilon^{3/2}v_t) \ll 1$, the system is to lowest order described by

$$\frac{v_\| + u}{qR}\frac{\partial f}{\partial \theta} = 0 \tag{4.3}$$

and, hence, f is to lowest order independent of θ. Thus, any poloidal variations in density, mean flow velocity or temperature must be small.

To determine the dependence of f on ψ_f, $v_{\|f}$ and μ, we define the transit average, which is the average over one orbit of a particle. For passing particles, the transit average is

$$\langle\mathcal{F}\rangle_\tau = \frac{1}{\tau}\int_0^{2\pi}\frac{\mathrm{d}\theta}{\dot{\theta}}\mathcal{F}, \tag{4.4}$$

where

$$\tau = \int_0^{2\pi} \frac{\mathrm{d}\theta}{\dot{\theta}}. \tag{4.5}$$

Using the approximate form of $\dot{\theta}$, the transit average for trapped particles is

$$\langle \mathcal{F} \rangle_\tau = \frac{qR}{\tau} \int_{-\theta_b}^{\theta_b} \frac{\mathrm{d}\theta}{v_\parallel + u} \mathcal{F}(v_\parallel + u > 0) + \frac{qR}{\tau} \int_{-\theta_b}^{\theta_b} \frac{\mathrm{d}\theta}{|v_\parallel + u|} \mathcal{F}(v_\parallel + u < 0), \tag{4.6}$$

where

$$\tau = 2qR \int_{-\theta_b}^{\theta_b} \frac{\mathrm{d}\theta}{|v_\parallel + u|} \tag{4.7}$$

and θ_b is the bounce angle, determined by $v_\parallel + u = 0$. Transit averaging (4.2) gives

$$\langle C[f, f] \rangle_\tau = -\langle \Sigma \rangle_\tau. \tag{4.8}$$

To lowest order in ϵ, the source $\langle \Sigma \rangle_\tau \sim \sqrt{\epsilon}\nu f$ is negligible, and the solution is a θ-independent Maxwellian in fixed-θ variables,

$$f_{M_f} = n(\psi_f) \left(\frac{m}{2\pi T(\psi_f)} \right)^{3/2} \exp\left(-\frac{m \left(v_{\parallel f} - V_\parallel(\psi_f) \right)^2}{2T(\psi_f)} - \frac{m\mu B_f}{T(\psi_f)} \right). \tag{4.9}$$

Note that unlike usual neoclassical theory, we keep the mean parallel velocity $V_\parallel \sim v_\parallel$. To this order particles do not leave their flux surface or experience a change in their parallel velocity going through one orbit, that is, $\psi \simeq \psi_f$ and $v_\parallel \simeq v_{\parallel f}$.

The dependence of T on ψ_f might be surprising because strong temperature gradients usually drive deviations away from a Maxwellian equilibrium. If the time scale associated with the ion energy flux Q, given by $nT/|\nabla\psi|(\partial Q/\partial\psi)$ is longer than the ion-ion collision time, and the orbit widths are of the same order as the transport barrier, there is no temperature gradient because all particles have reached thermodynamic equilibrium and have been able to sample the entire volume. This is why the temperature gradient was assumed to be small in (Kagan & Catto 2010; Catto *et al.* 2013). However, by having introduced the large aspect ratio expansion, the gradient lengths can be of the same size as the poloidal gyroradius whilst still being much larger than the ion orbit width. In this way, we can get a Maxwellian to lowest order and a strong temperature gradient at the same time.

We define the next order solution as

$$f = f_{M_f} + h(\psi_f, v_{\parallel f}, \mu) = f_M + g(\psi, \theta, v_\parallel, \mu), \tag{4.10}$$

where f_M is the Maxwellian in (4.9) evaluated at the particle variables $\psi, v_\parallel$ and μ,

$$f_M = n(\psi) \left(\frac{m}{2\pi T(\psi)} \right)^{3/2} \exp\left(-\frac{m \left(v_\parallel - V_\parallel(\psi) \right)^2}{2T(\psi)} - \frac{m\mu B(\psi, \theta)}{T(\psi)} \right). \tag{4.11}$$

At first order in ϵ one needs to be careful about the distinction between h and g. Whilst h is the distribution function in the fixed-θ variables and can be interpreted as the distribution of orbits, g is a function of the variables ψ, $v_\parallel$ and μ and it is the distribution function of particles in the classic sense.

In the banana regime, the collision frequency satisfies $qR\nu/v_t \ll \epsilon^{3/2}$. The collisionality is small enough that, in both the freely passing and the trapped-barely-passing region, orbits can be completed before particles collide. Consequently, h does not depend on θ to next order as $\dot{\theta}\partial h/\partial\theta \sim \epsilon^{1/2} v_t h/qR$, while $C[h, f_M] + C[f_M, h] \sim \nu h/\epsilon$. Thus, following

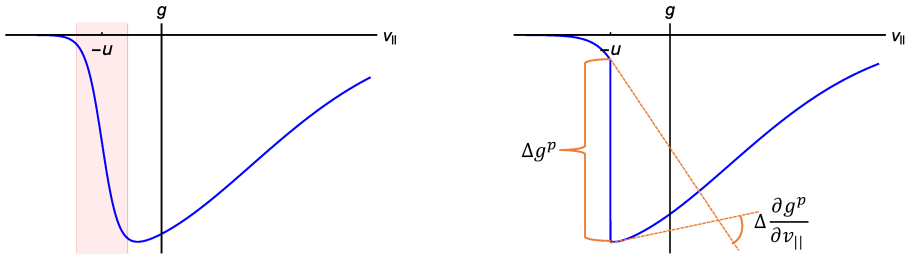

FIGURE 3. (a): This is a sketch of the distribution function g. The region of trapped-barely-passing particles (pink) is small. (b): The contribution coming from trapped-barely-passing particles is approximated as a discontinuity of the passing particle distribution function and its derivatives in velocity space.

(4.3), h does not depend on θ. The large aspect ratio expansion is crucial from here on. We expand $g = h + f_{M_f} - f_M$ in orders of $\sqrt{\epsilon}$,

$$g = g_0 + g_1 + ... \quad \text{where} \quad g_n \sim \epsilon^{\frac{n+1}{2}} f_M. \tag{4.12}$$

We will call the solution in the freely passing region, where $\left|v_{\|f} + u_f\right| \gg \sqrt{\epsilon} v_t$, the freely passing distribution function g^p, and the solution in the trapped-barely-passing region, where $\left|v_{\|f} + u_f\right| \sim \sqrt{\epsilon} v_t$, the trapped-barely-passing distribution function g^t. Note that, for convenience, we use the superscript t for the trapped-barely-passing region even though g^t also includes the distribution of barely-passing particles. The function g^t only exists in a small region of phase space, where $\left|v_{\|f} + u_f\right| \sim \sqrt{\epsilon} v_t$. Thus, the contribution of g^t can be interpreted as a discontinuity in g^p. We will find that it is sufficient to set $g \approx g^p$ in the entire phase space and determine from the solution for g^t the jump and derivative discontinuity conditions at $v_\| = -u$ for g^p. A sketch of g and how g^t is reduced to a discontinuity is shown in figure 3.

Within the trapped-barely-passing region we introduce the velocity variable $w \equiv v_\| + u \sim \sqrt{\epsilon} v_t$, which effectively stretches out the trapped-barely-passing region such that the boundary between the barely passing and the freely passing particles maps to $\pm\infty$. We require that the outer limiting solutions for g^t match the two inner limiting solutions of g^p, such that

$$g^t(w \to \infty) = g^p(v_\| \to -u^+) \qquad \text{and} \qquad g^t(w \to -\infty) = g^p(v_\| \to -u^-), \tag{4.13}$$

as well as

$$\left.\frac{\partial g^t}{\partial w}\right|_{w\to\infty} = \left.\frac{\partial g^p}{\partial v_\|}\right|_{v_\|\to -u^+} \qquad \text{and} \qquad \left.\frac{\partial g^t}{\partial w}\right|_{w\to-\infty} = \left.\frac{\partial g^p}{\partial v_\|}\right|_{v_\|\to -u^-}. \tag{4.14}$$

The jump condition at the trapped-passing boundary becomes

$$\Delta g^p = g_0^t(w \to \infty) - g_0^t(w \to -\infty). \tag{4.15}$$

In order for this jump to remain finite, the derivative of g_0^t must tend to zero at $\pm\infty$. The discontinuity condition in the derivatives thus requires the next order correction

$$\Delta\left(\frac{\partial g^p}{\partial v_\|}\right) = \left.\frac{\partial g_1^t}{\partial w}\right|_{w\to\infty} - \left.\frac{\partial g_1^t}{\partial w}\right|_{w\to-\infty}. \tag{4.16}$$

The jump and derivative discontinuity conditions follow from the solution of (4.8), for

which we need an expression for the collision operator. The lowest order solution is a Maxwellian, so we can linearise the collision operator around f_M using (4.10),

$$C[f,f] \simeq C[f_M,g] + C[g,f_M] \equiv C^{(l)}[g]. \tag{4.17}$$

Here, we have used that the collision operator acting on the Maxwellians vanishes. We neglect the smaller, nonlinear contribution $C[g,g]$. The linearised collision operator is

$$\begin{aligned} C^{(l)}[g] =& \lambda \boldsymbol{\nabla}_v \cdot \left[\int \mathrm{d}^3 v' f_M f'_M \boldsymbol{\nabla}_\omega \boldsymbol{\nabla}_\omega \omega \cdot \left(\boldsymbol{\nabla}_v \left(\frac{g}{f_M} \right) - \boldsymbol{\nabla}_{v'} \left(\frac{g'}{f'_M} \right) \right) \right] \\ =& \boldsymbol{\nabla}_v \cdot \left[f_M \boldsymbol{M} \cdot \boldsymbol{\nabla}_v \left(\frac{g}{f_M} \right) - \lambda f_M \int_{V_{\mathrm{tbp}}} \mathrm{d}^3 v' f'_M \boldsymbol{\nabla}_\omega \boldsymbol{\nabla}_\omega \omega \cdot \boldsymbol{\nabla}_{v'} \left(\frac{g^{t'}}{f'_M} \right) \right. \\ & \left. - \lambda f_M \int_{V_{\mathrm{p}}} \mathrm{d}^3 v' f'_M \boldsymbol{\nabla}_\omega \boldsymbol{\nabla}_\omega \omega \cdot \boldsymbol{\nabla}_{v'} \left(\frac{g^{p'}}{f'_M} \right) \right], \end{aligned} \tag{4.18}$$

where $\lambda = 2\pi Z^4 e^4 \log \Lambda / m^2$ and $\log \Lambda$ is the Coulomb logarithm. The integrals are over the trapped-barely-passing region V_{tbp} and the freely passing region V_{p}, respectively, and $\boldsymbol{\omega} = \boldsymbol{v} - \boldsymbol{v}'$. We have introduced the matrix

$$\boldsymbol{M} = \frac{\nu_\perp}{4} \left(|\boldsymbol{v} - V_\parallel \hat{\boldsymbol{b}}|^2 \boldsymbol{I} - (\boldsymbol{v} - V_\parallel \hat{\boldsymbol{b}})(\boldsymbol{v} - V_\parallel \hat{\boldsymbol{b}}) \right) + \frac{\nu_\parallel}{2} (\boldsymbol{v} - V_\parallel \hat{\boldsymbol{b}})(\boldsymbol{v} - V_\parallel \hat{\boldsymbol{b}}), \tag{4.19}$$

$$\nu_\perp = 3\sqrt{\frac{\pi}{2}} \nu \frac{\Xi(x) - \Psi(x)}{x^3}, \quad \nu_\parallel = 3\sqrt{\frac{\pi}{2}} \nu \frac{\Psi(x)}{x^3}, \quad \text{and} \quad \nu = \frac{4\sqrt{\pi} Z^4 e^4 n \log \Lambda}{3 T^{3/2} m^{1/2}}, \tag{4.20}$$

where $x = \sqrt{m/(2T)} |\boldsymbol{v} - V_\parallel \hat{\boldsymbol{b}}|$, $\Xi(x) = \mathrm{erf}(x) = (2/\sqrt{\pi}) \int_0^x \exp(-y^2) \mathrm{d}y$, $\Psi(x) = (\Xi - x\Xi')/(2x^2)$. The term proportional to $\nu_\perp$ describes pitch angle scattering and the term proportional to $\nu_\parallel$ represents energy diffusion.

We proceed to find the correction g. We expand (4.8) in orders of $\sqrt{\epsilon}$ and find to $O(\nu f_M/\sqrt{\epsilon})$ the jump condition Δg^p in section 4.1 and to $O(\nu f_M)$ the derivative discontinuity condition $\Delta(\partial g^p/\partial v_\parallel)$ in section 4.2. The distribution function g^p as well as poloidal variations of density and potential enter at $O(\sqrt{\epsilon}\nu f_M)$ and are presented in section 4.3 and section 4.4

4.1. *Jump condition*

The solution in the trapped-barely-passing region gives the jump and derivative discontinuity conditions for g^p. We start by finding an expression for the jump condition (4.15) by collecting terms of order $O(\nu f_M/\sqrt{\epsilon})$ in (4.8). The results of this subsection were already derived in a similar way by Shaing *et al.* (1994*a*). We reproduce the calculations to this order before presenting the higher order calculations where we find significant differences with previous work.

The equation to solve for g_0^t is

$$\langle C^{(l)}[g] \rangle_\tau = 0. \tag{4.21}$$

Changing to the fixed-θ variables and keeping only terms of $O(\nu f_M/\sqrt{\epsilon})$ of the collision operator in (4.18) yields

$$C^{(l)}[g] \simeq \boldsymbol{\nabla}_v w_f \cdot \frac{\partial}{\partial w_f} \left[f_M \boldsymbol{M} \cdot \boldsymbol{\nabla}_v w_f \frac{\partial (g^t/f_M)}{\partial w_f} \right]. \tag{4.22}$$

Only the derivatives with respect to $w_f \equiv v_{\parallel f} + u_f$ are kept because they are larger than the other velocity derivatives by $1/\sqrt{\epsilon}$. This is because in the trapped-barely-passing

region $w_f \sim \sqrt{\epsilon} v_t$ and hence we assume $\partial g^t/\partial w_f \sim g^t/(\sqrt{\epsilon} v_t)$. Using fixed-$\theta$ variables is also convenient because the matching between the trapped-barely-passing and freely passing region will hold for all θ. It follows from (A 17) that

$$\boldsymbol{\nabla}_v w_f = \frac{[w + Su\,(B_f/B - 1)]\,\hat{\boldsymbol{b}} - S\,(B_f/B - 1)\,\boldsymbol{v}_\perp}{w_f} \simeq \frac{w}{w_f}\hat{\boldsymbol{b}}. \tag{4.23}$$

Thus, the linear collision operator to lowest order is

$$C^{(l)}[g] \simeq \frac{w}{w_f}\frac{\partial}{\partial w_f}\left[M_\parallel \frac{w}{w_f}\frac{\partial g_0^t}{\partial w_f}\right], \tag{4.24}$$

where we have introduced the parallel component of $\boldsymbol{M}$

$$M_\parallel \equiv \hat{\boldsymbol{b}} \cdot \boldsymbol{M} \cdot \hat{\boldsymbol{b}} \simeq \frac{\nu_\perp}{2}\mu B + \frac{\nu_\parallel}{2}(u + V_\parallel)^2. \tag{4.25}$$

Here, we have used that $v_\parallel \simeq -u$ for trapped-barely-passing particles. The collision frequencies $\nu_\parallel$ and $\nu_\perp$ are evaluated at $x \simeq \sqrt{m[(u+V_\parallel)^2 + 2\mu B]/(2T)}$.

To determine g_0^t, we use (4.10) and expand the lowest order solution around a Maxwellian in the variables $(\psi, v_\parallel, \mu)$

$$f = f_{M_f} + h(\psi_f, v_{\parallel f}, \mu) \simeq f_M + (\psi_f - \psi)\left[\frac{\partial}{\partial\psi}\ln p + \frac{m(v_\parallel - V_\parallel)}{T}\frac{\partial V_\parallel}{\partial\psi}\right.$$
$$\left. + \left(\frac{m(v_\parallel - V_\parallel)^2}{2T} + \frac{m\mu B}{T} - \frac{5}{2}\right)\frac{\partial}{\partial\psi}\ln T\right] f_M - \frac{m(v_\parallel - V_\parallel)}{T}(v_{\parallel f} - v_\parallel) f_M + h(\psi, v_\parallel, \mu). \tag{4.26}$$

This result can be rewritten using the velocity variable $w = v_\parallel + u$, the relations (A 16), and the fact that $v_\parallel \simeq -u$ in the trapped-barely-passing region,

$$f \simeq f_M - \frac{I}{S\Omega}(w - w_f)\,\mathcal{D} f_M(v_\parallel = -u) + h, \tag{4.27}$$

where we have defined

$$\mathcal{D} = \frac{\partial}{\partial\psi}\ln p - \frac{m(u + V_\parallel)}{T}\left(\frac{\partial V_\parallel}{\partial\psi} - \frac{\Omega}{I}\right) + \left(\frac{m(u+V_\parallel)^2}{2T} + \frac{m\mu B}{T} - \frac{5}{2}\right)\frac{\partial}{\partial\psi}\ln T. \tag{4.28}$$

To avoid cluttering our notation, we will not distinguish between fixed-θ variables and $(\psi, v_\parallel, \mu)$ in most terms as they are almost the same. We will only keep the distinction between the two types of variables in places where they appear subtracted from each other, e.g. when we need $v_\parallel - v_{\parallel f}$ or $\psi - \psi_f$.

One can define the auxiliary function $\bar{h}$, which is a function of fixed-θ variables only, as

$$\bar{h} = h + \frac{I}{\Omega}\frac{w_f}{S}\mathcal{D} f_M(v_\parallel = -u), \tag{4.29}$$

and with that we find

$$g_0^t = \bar{h} - \frac{I}{\Omega}\frac{w}{S}\mathcal{D} f_M(v_\parallel = -u). \tag{4.30}$$

The trapped-barely-passing region contains both barely-passing particles and trapped particles and we need to distinguish between the two. The trapped-barely-passing bound-

ary for ions trapped on the low (high) field side for $S > 0$ ($S < 0$) and $\theta_f = 0$ is

$$w_{\rm tpb}^2 = 4S\left[\left(\mu B + u^2\right)\frac{r}{R} - \frac{Ze\phi_c}{m}\right]. \tag{4.31}$$

The trapped-barely-passing boundary for ions trapped on the low (high) field side for $S > 0$ ($S < 0$) and $\theta_f = \pi$ is

$$w_{\rm tpb}^2 = 4S\left[\frac{Ze\phi_c}{m} - \left(\mu B + u^2\right)\frac{r}{R}\right]. \tag{4.32}$$

A more detailed discussion about the distinction between the two cases, is presented in Appendix D. For barely-passing particles, for which $w_f^2 \geqslant w_{\rm tpb}^2$ holds, one can change from transit averages to flux surface averages by using that

$$\left\langle \frac{w}{w_f}(...)\right\rangle_\tau = \frac{1}{\tau}\int \frac{{\rm d}\theta}{w} qR \frac{w}{w_f}(...) = \frac{2\pi qR}{\tau w_f}\langle ...\rangle_\psi \tag{4.33}$$

where $\langle ...\rangle_\psi = 1/(2\pi)\int {\rm d}\theta(...)$ is the flux surface average. Then, using expression (4.30) and $(\partial w/\partial w_f) \simeq w_f/w$, the transit averaged collision operator becomes

$$\langle C^{(l)}[g]\rangle_\tau \simeq \frac{2\pi qR}{\tau w_f}\frac{\partial}{\partial w_f}\left\{ M_\parallel \left[\frac{\langle w\rangle_\psi}{w_f}\frac{\partial \bar{h}}{\partial w_f} - \frac{I}{\Omega S}\mathcal{D} f_M(v_\parallel = -u)\right]\right\}. \tag{4.34}$$

For trapped particles, which obey $w_f^2 \leqslant w_{\rm tpb}^2$, the contribution $g_0^t - \bar{h}$ is odd in w and hence it follows from (4.6) and (4.30) that

$$\begin{aligned}\langle C^{(l)}[g-\bar{h}]\rangle_\tau &= -\left\langle \frac{w}{w_f}\frac{\partial}{\partial w_f}\left[M_\parallel \frac{I}{\Omega S}\mathcal{D} f_M(v_\parallel = -u)\right]\right\rangle_\tau \\ &= \frac{1}{\tau}\int_{-\theta_b}^{\theta_b}\frac{{\rm d}\theta}{w_f} qR \frac{\partial}{\partial w_f}\left[M_\parallel \frac{I}{\Omega S}\mathcal{D} f_M(v_\parallel = -u)\right] \\ &\quad - \frac{1}{\tau}\int_{-\theta_b}^{\theta_b}\frac{{\rm d}\theta}{w_f} qR \frac{\partial}{\partial w_f}\left[M_\parallel \frac{I}{\Omega S}\mathcal{D} f_M(v_\parallel = -u)\right] = 0.\end{aligned} \tag{4.35}$$

It then follows from (4.21) and (4.34) that

$$M_\parallel \frac{\tau\langle w^2\rangle_\tau}{w_f}\frac{\partial \bar{h}}{\partial w_f} = K, \tag{4.36}$$

where K is a constant. $M_\parallel$ is constant in w_f and

$$\frac{\tau\langle w^2\rangle_\tau}{w_f} = qR\int_{-\theta_b}^{\theta_b}{\rm d}\theta\frac{w}{w_f} = qR\int_{-\theta_b}^{\theta_b}{\rm d}\theta\sqrt{1-\kappa^2\sin^2(\theta/2)}, \tag{4.37}$$

where κ^2 is defined in (D 4), such that for $w_f \to 0$, $\kappa^2 \to \infty$ as $\theta_b \to 0$. Hence, $\tau\langle w^2\rangle_\tau/w_f \to 0$ for $w_f \to 0$ and consequently $K = 0$ and $\partial\bar{h}/\partial w_f = 0$. For trapped particles, we find from (4.30) that

$$\frac{\partial g_0^t}{\partial w_f} = -\frac{I}{\Omega S}\frac{w_f}{w}\mathcal{D} f_M(v_\parallel = -u). \tag{4.38}$$

The contribution $\langle C^{(l)}[g-\bar{h}]\rangle_\tau$ is not zero for barely-passing particles because particles do not bounce, so there is no change in the sign of w and thus the transit average of a function that is odd in w does not vanish. Using equation (4.34) with the boundary

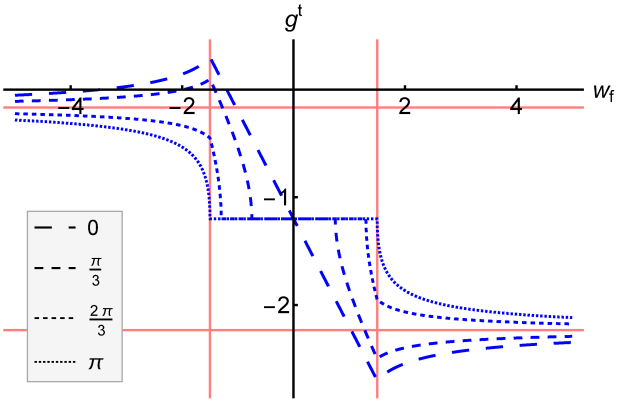

FIGURE 4. The distribution function g^t in the trapped and barely-passing region is symmetric around $w = 0$ and goes towards the same constants for any value of θ at $w \to \pm\infty$. Here, we chose $Iv_t\mathcal{D}f_M(v_\parallel = -u)/(\Omega S) = 1$, $g(\psi_f, w_f = 0, \mu) = -1.2$, $w_{\mathrm{tpb}} = \pm 1.5$, and w_f is in units of thermal velocity. The jump is $\Delta g^p = -2.0685$.

condition $\partial g_0^t/\partial w_f \to 0$ for $w_f \to \infty$, we find that the derivative of the distribution function for barely-passing particles is

$$\frac{\partial g_0^t}{\partial w_f} = \frac{I}{\Omega S}\left(\frac{w_f}{\langle w\rangle_\psi} - \frac{w_f}{w}\right)\mathcal{D}f_M(v_\parallel = -u), \tag{4.39}$$

where we have used $\partial w/\partial w_f \simeq w_f/w$. For the jump condition (4.15) we need to integrate (4.38) and (4.39) over w_f. We will show in section 4.3 that in the freely passing particle region, the distribution function is independent of θ to lowest order and hence the jump condition must be independent of θ as well. Thus, the jump condition must satisfy

$$\Delta g^p = \int_{-\infty}^{\infty} \mathrm{d}w_f \, \frac{\partial g_0^t}{\partial w_f} = \left\langle \int_{-\infty}^{\infty} \mathrm{d}w_f \, \frac{\partial g_0^t}{\partial w_f} \right\rangle_\psi . \tag{4.40}$$

We calculate this integral in Appendix D using the potential $\phi_\theta = \phi_c \cos\theta$ (see section 4.4). The final result is

$$\Delta g^p = -2.758 \frac{I}{\Omega S}\sqrt{\left|S\left[(\mu B + u^2)\frac{r}{R} - \frac{Ze}{m}\phi_c\right]\right|}\mathcal{D}f_M(v_\parallel = -u). \tag{4.41}$$

The distribution function g^t in (B 1) can be plotted using the integrals from Appendix D. The results for different values of θ are shown in figure 4. We find that the derivative is discontinuous at the trapped-passing boundary, and that the jump (4.41) is the same for any value of θ.

4.2. *Derivative discontinuity condition*

We proceed to derive an expression for the discontinuity condition (4.16). For the jump condition, we have to consider terms of $O(\nu f_M/\sqrt{\epsilon})$. For the derivative discontinuity condition, we still consider the trapped-barely-passing particles but need to go to higher order in $\sqrt{\epsilon}$ and collect terms of $O(\nu f_M)$. Going back to (4.21), we perform the change of variables in the collision operator (4.18) and only keep terms of $O(\nu f_M)$ or larger to

get

$$C^{(l)}[g] \simeq \frac{1}{\mathcal{J}}\frac{\partial}{\partial w_f}\left[\mathcal{J} f_M \boldsymbol{\nabla}_v w_f \cdot \boldsymbol{M}\cdot\boldsymbol{\nabla}_v\left(\frac{g^t}{f_M}\right)\right] + \frac{1}{\mathcal{J}}\frac{\partial}{\partial \mu}\left[\mathcal{J} f_M \boldsymbol{\nabla}_v \mu \cdot \boldsymbol{M}\cdot\boldsymbol{\nabla}_v w_f \frac{\partial (g_0^t/f_M)}{\partial w_f}\right] + \frac{1}{\mathcal{J}}\frac{\partial}{\partial \psi_f}\left[\mathcal{J} f_M \boldsymbol{\nabla}_v \psi_f \cdot \boldsymbol{M}\cdot\boldsymbol{\nabla}_v w_f \frac{\partial (g_0^t/f_M)}{\partial w_f}\right], \tag{4.42}$$

where

$$\mathcal{J} = \det\left(\frac{\partial(\boldsymbol{r},\boldsymbol{v})}{\partial(\psi_f,\theta,\zeta,w_f,\mu,\varphi)}\right) \simeq \frac{1}{\boldsymbol{B}\cdot\boldsymbol{\nabla}\theta}\frac{1}{\boldsymbol{\nabla}_v w_f\cdot(\boldsymbol{\nabla}_v\mu\times\boldsymbol{\nabla}_v\varphi)} \simeq \frac{qRw_f}{w} \tag{4.43}$$

is the Jacobian (note that we used (4.23) to obtain the last equality), φ is the gyroangle with $\nabla_v\varphi = \hat{\boldsymbol{b}}\times\boldsymbol{v}/v_\perp^2$ and

$$\boldsymbol{\nabla}_v\mu = \frac{\boldsymbol{v}_\perp}{B}, \qquad \boldsymbol{\nabla}_v\psi_f = \boldsymbol{\nabla}_v(\psi_f-\psi) \simeq \frac{I}{\Omega S}\left(\frac{w}{w_f}-1\right)\hat{\boldsymbol{b}}, \tag{4.44}$$

for which we have used (A 16). The Maxwellians in the second and third term of (4.42) are evaluated at $v_\parallel = -u$. Recall that the derivatives with respect to w_f are bigger by $1/\sqrt{\epsilon}$ than the derivatives with respect to μ and ψ_f.

We argued in (4.16) that the parallel velocity derivative of g_1^t is required for the derivative discontinuity condition. This derivative is of order $\sqrt{\epsilon}f_M$ and hence g_1^t only appears in the first term of (4.42), where the second derivative in parallel velocity of g_1^t produces a term of $O(\nu f_M)$. In all other terms that involve smaller derivatives with respect to μ and ψ_f, only g_0^t enters to this order. We show in Appendix C that taking the transit average of the collision operator yields

$$\langle C^{(l)}[g]\rangle_\tau \simeq \frac{1}{w_f\tau}\frac{\partial}{\partial w_f}\left[f_M w_f\tau\left\langle \boldsymbol{\nabla}_v w_f\cdot\boldsymbol{M}\cdot\boldsymbol{\nabla}_v\left(\frac{g^t}{f_M}\right)\right\rangle_\tau\right] + \frac{1}{w_f\tau}\frac{\partial}{\partial\mu}\left[2\mu f_M w_f\tau M_\perp\left\langle\frac{w}{w_f}\frac{\partial(g_0^t/f_M)}{\partial w_f}\right\rangle_\tau\right] + \frac{1}{w_f\tau}\frac{\partial}{\partial\psi_f}\left[f_M w_f\tau\frac{I}{\Omega S}M_\parallel\left\langle\left(\frac{w}{w_f}-1\right)\frac{w}{w_f}\frac{\partial(g_0^t/f_M)}{\partial w_f}\right\rangle_\tau\right] = 0. \tag{4.45}$$

Here, we introduced the component of $\boldsymbol{M}$

$$M_\perp \equiv \frac{\boldsymbol{v}_\perp}{|\boldsymbol{v}_\perp|^2}\cdot\boldsymbol{M}\cdot\hat{\boldsymbol{b}} \simeq (-u-V_\parallel)\left(-\frac{\nu_\perp}{4}+\frac{\nu_\parallel}{2}\right), \tag{4.46}$$

and set $v_\parallel = -u$ in the arguments of $\nu_\parallel$ and $\nu_\perp$, which is a good approximation in the trapped-barely-passing region.

The first term in equation (4.45) contains the derivative of g_1^t that is needed for the discontinuity condition. The distribution function for trapped-barely-passing particles, g^t, has to match with g^p at the boundary between the trapped-barely-passing region and the freely passing region, and thus

$$w_f\left\langle\boldsymbol{\nabla}_v w_f\cdot\boldsymbol{M}\cdot\boldsymbol{\nabla}_v\left(\frac{g^t}{f_M}\right)\right\rangle_\tau \simeq w\hat{\boldsymbol{b}}\cdot\boldsymbol{M}\cdot\boldsymbol{\nabla}_v\left(\frac{g^p}{f_M}\right) \tag{4.47}$$

for $w\to\pm\infty$. Hence, the solution for the discontinuity condition (4.16) in the banana

regime takes the form

$$\begin{aligned}
&\Delta\left[w\tau\hat{\boldsymbol{b}}\cdot\boldsymbol{M}\cdot\boldsymbol{\nabla}_v\left(\frac{g^p}{f_M}\right)\right]f_M \\
&=-\frac{\partial}{\partial\mu}\left[f_M\int_{-\infty}^{\infty}\mathrm{d}w_f\ w_f\tau 2\mu M_\perp\left\langle\frac{w}{w_f}\frac{\partial(g_0^t/f_M)}{\partial w_f}\right\rangle_\tau\right] \\
&\quad-\frac{\partial}{\partial\psi_f}\left[f_M\frac{I}{\Omega S}\int_{-\infty}^{\infty}\mathrm{d}w_f\ w_f\tau M_\parallel\left\langle\left(\frac{w}{w_f}-1\right)\frac{w}{w_f}\frac{\partial(g_0^t/f_M)}{\partial w_f}\right\rangle_\tau\right],
\end{aligned} \tag{4.48}$$

where we have multiplied (4.45) by $w_f\tau$ and integrated over w_f. Note that on the left hand side of the equation $w\tau\simeq 2\pi qR$. Following the steps in Appendix D.2 and recalling (4.40), we arrive at

$$\Delta\left[\hat{\boldsymbol{b}}\cdot\boldsymbol{M}\cdot\boldsymbol{\nabla}_v\left(\frac{g^p}{f_M}\right)\right]f_M=-\frac{\partial}{\partial\mu}\left(2\mu M_\perp\Delta g^p\right)+\frac{\partial}{\partial\psi_f}\left(\frac{I}{\Omega S}M_\parallel\Delta g^p\right), \tag{4.49}$$

where Δg^p is given in (4.41).

We have found the jump and derivative discontinuity conditions. Next, an equation for the freely passing region is derived which completes an approximate description of the entire velocity space.

4.3. *The freely passing region*

The freely passing particle distribution function enters to order $O(\sqrt{\epsilon}\nu f_M)$ in (4.8). The explicit expression of the collision operator in (4.18) is substituted into the simplified drift kinetic equation (4.8), which gives

$$\begin{aligned}
&\left\langle\boldsymbol{\nabla}_v\cdot\left[f_M\boldsymbol{M}\cdot\boldsymbol{\nabla}_v\left(\frac{g^p}{f_M}\right)-\lambda f_M\int_{V_\mathrm{p}}\mathrm{d}^3v' f'_M\boldsymbol{\nabla}_\omega\boldsymbol{\nabla}_\omega\omega\cdot\boldsymbol{\nabla}_{v'}\left(\frac{g^{p'}}{f'_M}\right)\right]\right\rangle_\tau \\
&-\lambda\left\langle\boldsymbol{\nabla}_v\cdot\left[f_M\int_{V_\mathrm{tbp}}\mathrm{d}^3v'\ f'_M\boldsymbol{\nabla}_\omega\boldsymbol{\nabla}_\omega\omega\cdot\boldsymbol{\nabla}_{v'}\left(\frac{g^{t'}}{f'_M}\right)\right]\right\rangle_\tau=-\langle\Sigma\rangle_\tau.
\end{aligned} \tag{4.50}$$

The distribution function $g\sim\sqrt{\epsilon}f_M$ and the gradient acting on $g^{t'}$ gives a factor of $1/\sqrt{\epsilon}v_t$. In the third term on the right hand side $\boldsymbol{\nabla}_{v'}g^{t'}\sim f_M/v_t$ and $V_\mathrm{tbp}\sim\sqrt{\epsilon}v_t^3$, so all three terms on the left hand side are of the order $O(\sqrt{\epsilon}\nu f_M)$.

We combine the first two terms in equation (4.50) and define the linearised freely passing collision operator

$$C_p^{(l)}[g]\equiv\boldsymbol{\nabla}_v\cdot\left[f_M\boldsymbol{M}\cdot\boldsymbol{\nabla}_v\left(\frac{g^p}{f_M}\right)-\lambda f_M\int_{V_\mathrm{p}}\mathrm{d}^3v' f'_M\boldsymbol{\nabla}_\omega\boldsymbol{\nabla}_\omega\omega\cdot\boldsymbol{\nabla}_{v'}\left(\frac{g^{p'}}{f'_M}\right)\right] \tag{4.51}$$

to write (4.50) as

$$\langle C_p^{(l)}[g]\rangle_\tau-\lambda\left\langle\boldsymbol{\nabla}_v\cdot\left[f_M\int_{V_\mathrm{tbp}}\mathrm{d}^3v'\ f'_M\boldsymbol{\nabla}_\omega\boldsymbol{\nabla}_\omega\omega\cdot\boldsymbol{\nabla}_{v'}\left(\frac{g^{t'}}{f'_M}\right)\right]\right\rangle_\tau=-\langle\Sigma\rangle_\tau. \tag{4.52}$$

This is the equation for the passing distribution function. Equation (4.52) has solvability conditions, which are the moment equations we calculate in section 5. To obtain the moment equations, the jump and derivative discontinuity conditions in equations (4.41) and (4.48) are needed.

We are interested in the poloidal variations of density, mean parallel flow velocity,

temperature, and electric potential, for which the θ-dependent part of g^p, $g^p - \langle g^p \rangle_\psi$, is of interest. We argued that h only depends on θ via the dependence of ψ_f and $v_{\parallel f}$ on θ. Since $g^p = h^p + f_{M_f} - f_M$ and $f_{M_f} - f_M \sim \epsilon f_M$, $g^p \simeq h^p$ to lowest order. The θ-dependent part of g^p is given by the next order,

$$\begin{aligned} & g^p - \langle g^p \rangle_\psi \simeq f_{M_f} - f_M - \langle f_{M_f} - f_M \rangle_\psi \\ & \simeq (\psi_f - \psi - \langle \psi_f - \psi \rangle_\psi) \frac{\partial f_M}{\partial \psi} + \left(v_{\parallel f} - v_\parallel - \langle v_{\parallel f} - v_\parallel \rangle_\psi \right) \frac{\partial f_M}{\partial v_\parallel} + \frac{m\mu}{T} \left(B - \langle B \rangle_\psi \right) f_M \\ & = - \frac{Ir}{\Omega R} \frac{\left(v_\parallel^2 + \mu B \right) \cos\theta - Ze\phi_\theta R/(mr)}{v_\parallel + u} \left[\frac{\partial}{\partial \psi} \ln p + \frac{m(v_\parallel - V_\parallel)}{T} \left(\frac{\partial V_\parallel}{\partial \psi} - \frac{\Omega}{I} \right) \right. \\ & \quad \left. + \left(\frac{m(v_\parallel - V_\parallel)^2}{2T} + \frac{m\mu B}{T} - \frac{5}{2} \right) \frac{\partial}{\partial \psi} \ln T \right] f_M - \frac{r}{R} \cos\theta \frac{m}{T} \left[v_\parallel (v_\parallel - V_\parallel) + \mu B \right] f_M, \end{aligned} \tag{4.53}$$

where we have used the relations (A 5) and (A 6) as well as $B_f/B - \langle B_f/B \rangle_\psi = (r/R)\cos\theta$. The $\theta-$dependent part of the distribution function is of $O(\epsilon f_M)$ and consequently the θ-independent part of g^p is bigger than $g^p - \langle g^p \rangle_\psi$ by order $\sqrt{\epsilon}$. In Appendix B we show that the θ dependent part of the solution for g_0^t matches with (4.53).

4.4. *Poloidal variations and electric potential*

In the tokamak core, trapped particles are located around $v_\parallel = 0$, and for a Maxwellian with $V_\parallel = 0$ the number of passing particles with $v_\parallel > 0$ and $v_\parallel < 0$ is the same to lowest order. The trapped-passing boundary in our ordering is shifted such that trapped particles are located around $v_\parallel = -u$. The lowest order distribution function is still a Maxwellian, but it has a mean parallel velocity $V_\parallel$. For $V_\parallel \neq -u$, this implies that the number of passing particles with $v_\parallel + u > 0$ and $v_\parallel + u < 0$ is different. This discrepancy causes a poloidal variation in density, mean parallel velocity, temperature and poloidal potential.

If, for example, the magnetic drifts are pointing downwards, as shown in figure 5, particles with a positive (negative) poloidal velocity are being pushed inwards (outwards) with respect to their flux surface at $\theta = 0$ and outwards (inwards) at $\theta = \pi$. Let us assume a density gradient such that there is higher density inside a flux surface than there is outside. In this case, there are more particles with positive poloidal velocity at $\theta = 0$ than there are particles with negative poloidal velocity (see figure 5a), because particles with positive poloidal velocity come from the high density region. At $\theta = \pi$, the opposite is true, because the orbits of particles with positive poloidal velocity come from the low density region (see figure 5b). In standard low flow neoclassical theory, the number of particles with positive and negative poloidal velocity is the same, so these effects cancel out and there is no poloidal variation in density. For a shifted trapped-passing boundary, the number of particles with positive and negative poloidal velocity are different and there is a poloidal variation of density within a flux surface. The same argument can be constructed for poloidal variation of temperature and mean parallel flow.

The small poloidal variation of density, n_θ, is

$$n_\theta(\psi, \theta) = \int \mathrm{d}^3 v \; g - \left\langle \int \mathrm{d}^3 v \; g \right\rangle_\psi . \tag{4.54}$$

The integration is over the entire range of the parallel velocity and hence over both, the trapped-barely-passing and freely passing regions. The freely passing region is the

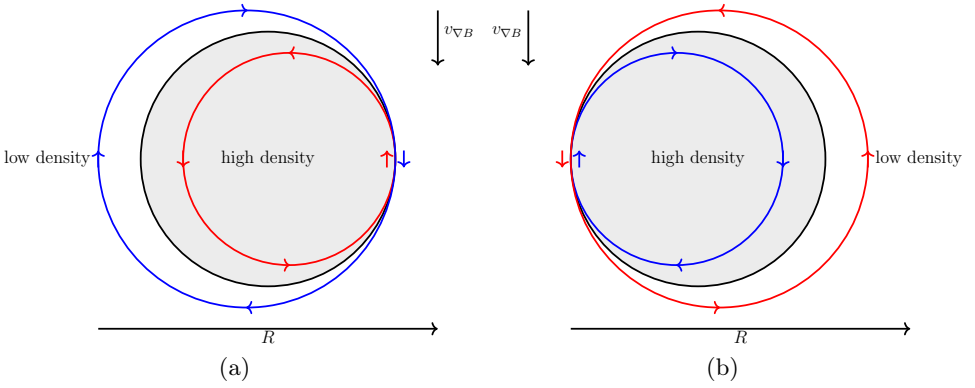

FIGURE 5. (a): At $\theta = 0$, particles with a positive poloidal velocity (red) are pushed inwards, completing their orbits through a region of higher density, and particles with a negative poloidal velocity (blue) are pushed outwards, completing their orbits through a region of lower density. Hence, red particles are more numerous than blue particles. (b): At $\theta = \pi$ on the same flux surface, the opposite is the case and there are fewer red particles than there are blue particles. If red particles are more numerous than blue particles and the density is higher at smaller radii, there will be a higher density at $\theta = 0$ than at $\theta = \pi$ and there is poloidal variation of density within a flux surface.

part of velocity space for which $v_\parallel$ is not close to $-u$. Importantly, the freely passing distribution function (4.53) diverges at $w = 0$. This divergence is picked up by the trapped distribution function g^t. As a result, the integration over phase space is split up into an integration over g^t in the trapped-barely-passing region and a principle value integral over g^p which captures the freely passing region while ignoring the divergence near $v_\parallel = -u$. Contribution from the divergence is accounted for by the integral of the distribution function g^t in the trapped-barely-passing region. For trapped particles, it follows directly from (B 1) that

$$\int \mathrm{d}\mu \int_{\text{trapped}} \mathrm{d}w\ 2\pi B g^t - \left\langle \int \mathrm{d}\mu \int_{\text{trapped}} \mathrm{d}w\ 2\pi B g^t \right\rangle_\psi = 0. \tag{4.55}$$

For barely passing and freely passing particles, the flux surface average of the density can be replaced by the integral over the flux surface averaged distribution function because the θ-dependence of B is small. Thus, (4.54) can be written as

$$n_\theta = \int \mathrm{d}\mu \int_{\text{barely-passing}} \mathrm{d}w\ 2\pi B(g^t - \langle g^t \rangle_\psi) + \int \mathrm{d}\mu \left[\mathrm{PV} \int \mathrm{d}v_\parallel\ 2\pi B(g^p - \langle g^p \rangle_\psi) \right], \tag{4.56}$$

where the first term only contains the barely-passing particles. However, this contribution vanishes to lowest order because $g_0^t - \langle g_0^t \rangle_\psi$ is odd in w, which follows from (B 10). The integration of the second term in equation (4.56) is performed in Appendix E, where the

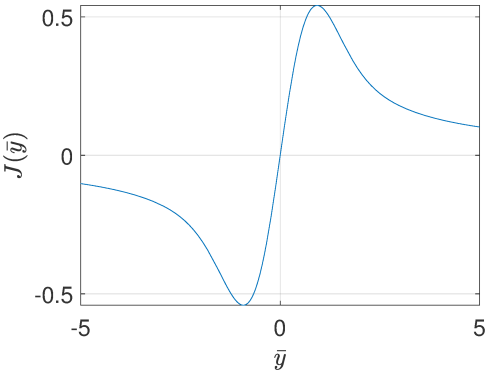

FIGURE 6. The function J defined in (4.58) as a function of $\bar{y} = \sqrt{m/(2T)}(u + V_\parallel)$.

θ-dependent part of the distribution function is taken from (4.53). The result is

$$n_\theta = -n\frac{Ir}{\Omega R}\left\{\sqrt{\frac{2T}{m}}J\left[\left(\frac{mV_\parallel^2}{T}\cos\theta + \cos\theta - \frac{Ze\phi_\theta R}{Tr}\right)\left(\frac{\partial}{\partial\psi}\ln p - \frac{3}{2}\frac{\partial}{\partial\psi}\ln T\right)\right.\right.$$
$$\left. + \cos\theta\frac{\partial}{\partial\psi}\ln T\right] + \left[1 - 2\sqrt{\frac{m}{2T}}(V_\parallel + u)J\right]\left\{(V_\parallel - u)\cos\theta\left(\frac{\partial}{\partial\psi}\ln p - \frac{3}{2}\frac{\partial}{\partial\psi}\ln T\right)\right.$$
$$- (V_\parallel + u)\left[\left(\frac{mV_\parallel^2}{2T} + \frac{1}{2}\right)\cos\theta - \frac{Ze\phi_\theta R}{2Tr}\right]\frac{\partial}{\partial\psi}\ln T + \left(\frac{\partial V_\parallel}{\partial\psi} - \frac{\Omega}{I}\right)\left[\left(\frac{mu^2}{T} + 1\right.\right.$$
$$\left.\left. - \frac{m(V_\parallel + u)^2}{T}\right)\cos\theta - \frac{Ze\phi_\theta R}{Tr}\right]\Bigg\} + \left[1 + 2\frac{m(V_\parallel + u)^2}{2T} - 4\left(\frac{m}{2T}\right)^{3/2}(V_\parallel + u)^3 J\right]$$
$$\left.\times\cos\theta\left(\frac{\partial V_\parallel}{\partial\psi} - \frac{\Omega}{I} + \frac{V_\parallel - u}{2}\frac{\partial}{\partial\psi}\ln T\right)\right\} - 2n\frac{r}{R}\cos\theta, \tag{4.57}$$

where we introduced the function

$$J = \frac{\sqrt{\pi}}{2}\exp\left(-\frac{m(u + V_\parallel)^2}{2T}\right)\mathrm{erfi}\left(\sqrt{\frac{m}{2T}}(u + V_\parallel)\right), \tag{4.58}$$

which is plotted in figure 6 and $\mathrm{erfi}(x) = (2/\sqrt{\pi})\int_0^x \exp(t^2)\mathrm{d}t$. The orbit width of passing particles is of order ϵ and hence the poloidal variations in density are of order ϵ as well.

The poloidal variation of density creates a poloidal variation in electric potential ϕ_θ that is determined via quasineutrality. Assuming a Boltzmann response of the electrons, the quasineutrality condition yields

$$Z\int \mathrm{d}^3v\ g - \left\langle Z\int \mathrm{d}^3v\ g\right\rangle_\psi = \frac{en_e}{T_e}\phi_\theta. \tag{4.59}$$

Looking at (4.57) we find that the potential has the form $\phi_\theta = \phi_c\cos\theta$, and the

quasineutrality condition (4.59) yields

$$\left\{\frac{en_e}{T_e}-\frac{Z^2neI}{T\Omega}\left[\sqrt{\frac{2T}{m}}J\left(\frac{\partial}{\partial\psi}\ln p-\frac{3}{2}\frac{\partial}{\partial\psi}\ln T\right)+\left[1-2\sqrt{\frac{m}{2T}}(V_\parallel+u)J\right]\left(\frac{\partial V_\parallel}{\partial\psi}-\frac{\Omega}{I}\right.\right.\right.$$
$$\left.\left.\left.-\frac{(V_\parallel+u)}{2}\frac{\partial}{\partial\psi}\ln T\right)\right]\right\}\phi_c=-Zn\frac{Ir}{\Omega R}\left\{\sqrt{\frac{2T}{m}}J\left[\left(\frac{mV_\parallel^2}{T}+1\right)\left(\frac{\partial}{\partial\psi}\ln p-\frac{3}{2}\frac{\partial}{\partial\psi}\ln T\right)\right.\right.$$
$$\left.+\frac{\partial}{\partial\psi}\ln T\right]+\left[1-2\sqrt{\frac{m}{2T}}(V_\parallel+u)J\right]\left[(V_\parallel-u)\left(\frac{\partial}{\partial\psi}\ln p-\frac{3}{2}\frac{\partial}{\partial\psi}\ln T\right)\right.$$
$$+\left(\frac{\partial V_\parallel}{\partial\psi}-\frac{\Omega}{I}\right)\left(\frac{mu^2}{T}+1-\frac{m(V_\parallel+u)^2}{T}\right)-\frac{V_\parallel+u}{2}\left(\frac{mV_\parallel^2}{T}+1\right)\frac{\partial}{\partial\psi}\ln T\Bigg]$$
$$\left.+\left[1+2\frac{m}{2T}(V_\parallel+u)^2-4\left(\frac{m}{2T}\right)^{3/2}(V_\parallel+u)^3J\right]\left(\frac{\partial V_\parallel}{\partial\psi}-\frac{\Omega}{I}+\frac{V_\parallel-u}{2}\frac{\partial}{\partial\psi}\ln T\right)\right\}$$
$$-2Zn\frac{r}{R}. \tag{4.60}$$

For $\phi_c>0$, the maximum of the potential is on the low-field side of the plasma, so the potential can trap particles on the high-field side for $S>0$. For $\phi_c<0$ and $S>0$, the potential reaches its maximum on the high field side and it can trap particles on the low-field side if electrostatic trapping dominates over magnetic trapping and centrifugal force.

Charge exchange recombination spectroscopy measurements in both Alcator C-Mod (Churchill *et al.* 2015; Theiler *et al.* 2014) and ASDEX-Upgrade (Cruz-Zabala *et al.* 2022) have observed poloidal variations in impurity density and temperatures in the pedestal of H-mode plasmas. These experiments also demonstrated that the main ion temperature and radial electric field cannot simultaneously be flux functions. This is consistent with our calculation and argumentation of poloidal variations of the electric potential and density.

We have found expressions for the distribution function in the passing region and the jump and derivative discontinuity condition given by the trapped-barely-passing region, and we have found the form of the poloidally varying component of the electric potential. These expressions are needed to calculate the solvability conditions for (4.52).

5. Moment equations

In order to study the transport in the pedestal, we want to find particle, parallel momentum and energy fluxes and how they give rise to profiles of n, T, u, $V_\parallel$ and ϕ_c. First, we integrate (4.52), for which the jump and derivative discontinuity conditions are required, and find the solvability conditions, which are the equations for particle, parallel momentum and energy conservation.

The full derivation is explained in Appendix F, where we show that the particle conservation equation

$$\frac{\partial}{\partial\psi_f}\left(-\frac{I}{\Omega m}F_\parallel\right)=\int \mathrm{d}^3v_f\ \langle\Sigma\rangle_\tau, \tag{5.1}$$

is the result of integrating (4.52) over velocity space. Here,

$$F_\parallel = -\int \mathrm{d}\mu \; \frac{2\pi m B}{S} M_\parallel \Delta g^p \tag{5.2}$$

is the parallel force due to the friction between passing and trapped particles, and Δg^p is the jump condition given in (4.41). The integration over $\mathrm{d}^3 v_f$ is an integration over velocity space in the fixed-θ variables, where $\mathrm{d}^3 v_f = 2\pi B \, \mathrm{d}\mu \, \mathrm{d}v_{\parallel f}$. The integration eliminated the contribution from the freely passing particle distribution g^p to the particle transport and for this reason is a solvbility condition: it must be satisfied regardless of the value of g^p. Trapped and barely passing particles dominate transport as we have estimated in section 2. We define the particle flux Γ as

$$\frac{\partial \Gamma}{\partial \psi_f} = \left\langle \int \mathrm{d}^3 v_f \; \Sigma \right\rangle_\psi . \tag{5.3}$$

The term on the left hand side of (5.1) is the divergence of a particle flux and the term on the right hand side is a source of particles. It follows directly from (5.1) and (5.3) that the neoclassical ion particle flux is

$$\Gamma = -\frac{I}{m\Omega} F_\parallel . \tag{5.4}$$

The parallel force $F_\parallel$ can drive a radial particle flux via an effect similar to the one that gives the Ware pinch (Ware 1970).

The parallel momentum equation is the result of multiplying (4.52) by $m v_{\parallel f}$ and integrating over velocity space. The equation becomes

$$\frac{\partial}{\partial \psi_f} \left(\frac{I}{\Omega} u F_\parallel \right) + F_\parallel = \gamma, \tag{5.5}$$

where $\gamma = \int \mathrm{d}^3 v \; m v_{\parallel f} \langle \Sigma \rangle_\tau$ is the parallel momentum input per unit volume. The calculation that leads to (5.5) is presented in Appendix F.2. We can use the particle flux (5.4) in (5.5) and arrive at

$$\frac{\partial}{\partial \psi_f} \left(m u \Gamma \right) + \frac{m\Omega}{I} \Gamma = -\gamma, \tag{5.6}$$

which is a relation purely between the particle flux, parallel momentum input and u. The first term on the left hand side of (5.6) is the flux of parallel momentum carried by the trapped particles. The second term on the left is the force due to the friction between trapped and passing particles. The term on the right hand side of the equation is a source of parallel momentum.

As for the particle and parallel momentum equations, one can find the energy equation by multiplying (4.52) by $m v_f^2/2$ and integrating over velocity space to arrive at

$$\frac{\partial}{\partial \psi_f} \left(\frac{IT}{m\Omega} \Theta \right) - u F_\parallel = \int \mathrm{d}^3 v_f \; \frac{m v_f^2}{2} \langle \Sigma \rangle_\tau , \tag{5.7}$$

where

$$\Theta = \int \mathrm{d}\mu \; \frac{2\pi m B}{S} \left(\frac{m\mu B}{T} + \frac{m u^2}{2T} \right) M_\parallel \Delta g^p . \tag{5.8}$$

The energy flux Q is defined similarly to Γ as

$$\frac{\partial Q}{\partial \psi_f} - Ze\Gamma \frac{\partial \phi}{\partial \psi_f} = \left\langle \int \mathrm{d}^3 v_f \ \frac{m v_f^2}{2} \Sigma \right\rangle_\psi . \tag{5.9}$$

A comparison to (5.7) gives

$$Q = \frac{TI}{m\Omega}\Theta. \tag{5.10}$$

The flux of energy on the left hand side of (5.7) contains both convective energy flux, which is the energy carried by the particle flux, and a conduction energy flux. The second term on the left of (5.9) is the work done by the radial electric field. The term on the right represents energy injection.

The same equations for particle, parallel momentum and energy (5.1), (5.5) and (5.7) can be found using moments of the original Fokker-Planck kinetic equation. At this point we can switch from fixed-θ variables to normal variables and drop the subscript f because the difference is small in ϵ.

We can substitute (4.25) for $M_\parallel$ and the jump condition (4.41) into (5.2) to find the particle flux from (5.4)

$$\begin{aligned}\Gamma = &- 2.758 \frac{I^2 \pi B}{|S|^{3/2}\Omega^2} n \left(\frac{m}{2\pi T}\right)^{3/2} \sqrt{\frac{T}{m}} \int \mathrm{d}\mu \exp\left(-\frac{m(u+V_\parallel)^2}{2T} - \frac{m\mu B}{T}\right) \\ &\times \sqrt{\left|\left(\frac{m\mu B}{T} + \frac{mu^2}{T}\right)\frac{r}{R} - \frac{Ze}{T}\phi_c\right|} \left(\nu_\perp \mu B + \nu_\parallel (u+V_\parallel)^2\right) \mathcal{D}.\end{aligned} \tag{5.11}$$

Integration over $x = \sqrt{m\mu B/T + m(u+V_\parallel)^2/(2T)}$ gives the final form of Γ,

$$\begin{aligned}\Gamma = -1.102 \sqrt{\frac{r}{R}} \frac{\nu I^2 p}{|S|^{3/2} m \Omega^2} \Bigg\{ &\left[\frac{\partial}{\partial \psi} \ln p - \frac{m(u+V_\parallel)}{T}\left(\frac{\partial V_\parallel}{\partial \psi} - \frac{\Omega}{I}\right)\right] G_1(\bar{y},\bar{z}) \\ &- 1.17 \frac{1}{T}\frac{\partial T}{\partial \psi} G_2(\bar{y},\bar{z})\Bigg\},\end{aligned} \tag{5.12}$$

where $\bar{y} = \sqrt{m/(2T)}(u+V_\parallel)$, $\bar{z} = mu^2/T - Ze\phi_c R/(Tr)$,

$$G_1(\bar{y},\bar{z}) \equiv \frac{\int_{|\bar{y}|}^\infty \mathrm{d}x \ k(x,\bar{y},\bar{z})}{\int_0^\infty \mathrm{d}x \ 0.5 x e^{-x^2} \left[\Xi(x) - \Psi(x)\right]} = 7.51 \int_{|\bar{y}|}^\infty \mathrm{d}x \ k(x,\bar{y},\bar{z}), \tag{5.13}$$

$$\begin{aligned} G_2(\bar{y},\bar{z}) &\equiv \frac{\int_{|\bar{y}|}^\infty \mathrm{d}x \left(x^2 - 5/2\right) k(x,\bar{y},\bar{z})}{\int_0^\infty \mathrm{d}x \ 0.5x \left(x^2 - 5/2\right) e^{-x^2} \left[\Xi(x) - \Psi(x)\right]} \\ &= -6.40 \int_{|\bar{y}|}^\infty \mathrm{d}x \left(x^2 - \frac{5}{2}\right) k(x,\bar{y},\bar{z}),\end{aligned} \tag{5.14}$$

and

$$k(x,\bar{y},\bar{z}) = \sqrt{|x^2 + \bar{z} - \bar{y}^2|} e^{-x^2} \left\{ \left(\frac{1}{2} - \frac{\bar{y}^2}{2x^2}\right)\left[\Xi(x) - \Psi(x)\right] + \frac{\bar{y}^2}{x^2}\Psi(x)\right\}. \tag{5.15}$$

The functions G_1 and G_2 are normalised to recover the standard neoclassical results when $\bar{y} = 0 = \bar{z}$, $G_1(0,0) = 1 = G_2(0,0)$. We note that the term in (5.12) proportional to $[V_\parallel - (-u)]\Omega/I$ is particle flux due to the parallel friction between trapped particles located

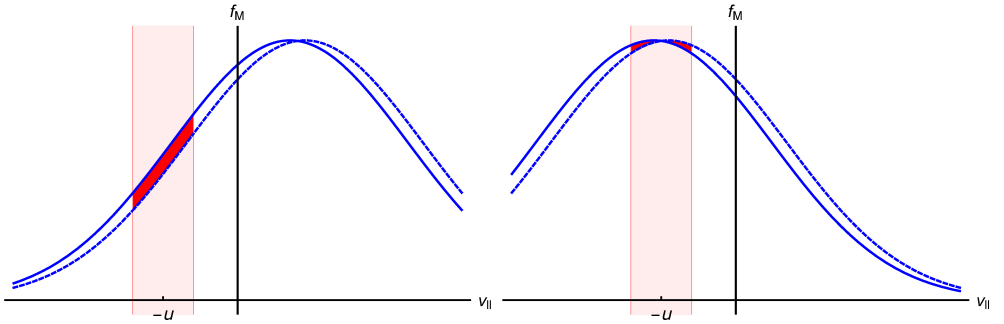

FIGURE 7. (a): A small shift in $V_\parallel$ for $V_\parallel$ not close to $-u$ going from one surface (solid line) to another flux surface (dashed line) causes a strong change of the number of trapped particles (red area between curves) in the trapped-barely-passing region (pink). (b): A small shift in $V_\parallel$ for $V_\parallel$ close to $-u$ gives only a small change in the number of trapped-barely-passing particles (red areas between curves cancel) in the trapped-barely-passing region.

around $-u$ and the passing particles with a mean velocity $V_\parallel$. The term proportional to $(u + V_\parallel)\partial V_\parallel/(\partial\psi)$ is related to a shift in the Maxwellian and hence of the density gradient in the trapped region if the Maxwellian is not centered around the trapped region, i.e. if $V_\parallel + u$ is not small (see figure 7). The remaining terms include the pressure and temperature gradients that usually drive radial particle flux but here are modified by the integrals G_1 and G_2. Note that the poloidal potential affects transport as it enters in $\bar{z}$.

Similarly, Q is

$$Q = \frac{mu^2}{2}\Gamma - 1.463\sqrt{\frac{r}{R}}\frac{\nu I^2 pT}{|S|^{3/2} m\Omega^2}\left\{\left[\frac{\partial}{\partial\psi}\ln p - \frac{m(u+V_\parallel)}{T}\left(\frac{\partial V_\parallel}{\partial\psi} - \frac{\Omega}{I}\right)\right] H_1(\bar{y},\bar{z}) - 0.25\frac{1}{T}\frac{\partial T}{\partial\psi}H_2(\bar{y},\bar{z})\right\}, \tag{5.16}$$

where

$$H_1(\bar{y},\bar{z}) \equiv \frac{\int_{|\bar{y}|}^\infty \mathrm{d}x\,\left(x^2-\bar{y}^2\right)k(x,\bar{y},\bar{z})}{\int_0^\infty \mathrm{d}x\;0.5x^3 e^{-x^2}[\Xi(x)-\Psi(x)]} = 5.66\int_{|\bar{y}|}^\infty \mathrm{d}x\,\left(x^2-\bar{y}^2\right)k(x,\bar{y},\bar{z}) \tag{5.17}$$

and

$$\begin{aligned} H_2(\bar{y},\bar{z}) &\equiv \frac{\int_{|\bar{y}|}^\infty \mathrm{d}x\,\left(x^2-\bar{y}^2\right)\left(x^2-5/2\right)k(x,\bar{y},\bar{z})}{\int_0^\infty \mathrm{d}x\;0.5x^3\left(x^2-5/2\right)e^{-x^2}[\Xi(x)-\Psi(x)]} \\ &= -22.63\int_{|\bar{y}|}^\infty \mathrm{d}x\,\left(x^2-\bar{y}^2\right)\left(x^2-\frac{5}{2}\right)k(x,\bar{y},\bar{z}). \end{aligned} \tag{5.18}$$

Again, we introduce a convenient normalisation such that $H_1(0,0) = 1 = H_2(0,0)$ in the standard neoclassical limit. We have found explicit expressions for particle (5.1), parallel momentum (5.5) and energy conservation (5.7).

Next, we want to compare our results to previous work. First, we take the high flow and low flow neoclassical limit, and then we give a comparison of our results to those by Catto *et al.* (2013) and Shaing & Hsu (2012).

In the high flow regime of the usual neoclassical theory (Hinton & Wong 1985), $V_\parallel + u$ and all gradients as well as source terms are small. If we take this limit in (5.6) and assume that the source of parallel momentum γ is small, we find that

$$\Gamma = 0, \tag{5.19}$$

which is consistent with the usual result in the high-flow regime (Hinton & Wong 1985; Catto *et al.* 1987). Using the particle flux equation (5.12), $\bar{\Gamma} = 0$ gives

$$\frac{\partial}{\partial \psi} \ln p + \frac{m\Omega(V_\parallel + u)}{IT} = 1.17 \frac{G_2(\bar{y}, \bar{z})}{G_1(\bar{y}, \bar{z})} \frac{\partial}{\partial \psi} \ln T. \tag{5.20}$$

We can use this in (5.16) to get the high flow energy flux

$$Q = -1.71 \sqrt{\frac{r}{R}} \frac{I^2 \nu T p}{m\Omega^2} \Delta\bar{Q} \frac{\partial}{\partial \psi} \ln T, \tag{5.21}$$

where

$$\Delta\bar{Q} \equiv \frac{H_1(\bar{y}, \bar{z}) G_2(\bar{y}, \bar{z}) - 0.21 H_2(\bar{y}, \bar{z}) G_1(\bar{y}, \bar{z})}{G_1(\bar{y}, \bar{z})} \geqslant 0. \tag{5.22}$$

The quantity $\Delta\bar{Q}$ is positive, which follows from

$$\Delta\bar{Q} = -4.82 \frac{\left(\int_{|\bar{y}|}^\infty \mathrm{d}x \; x^2 k(x, \bar{y}, \bar{z}) \right)^2 - \int_{|\bar{y}|}^\infty \mathrm{d}x \; k(x, \bar{y}, \bar{z}) \int_{|\bar{y}|}^\infty \mathrm{d}x \; x^4 k(x, \bar{y}, \bar{z})}{\int_{|\bar{y}|}^\infty \mathrm{d}x \; k(x, \bar{y}, \bar{z})} \tag{5.23}$$

and the Cauchy-Schwarz inequality

$$\left(\int_{|\bar{y}|}^\infty \mathrm{d}x \; x^2 k(x, \bar{y}, \bar{z}) \right)^2 \leqslant \int_{|\bar{y}|}^\infty \mathrm{d}x \; k(x, \bar{y}, \bar{z}) \int_{|\bar{y}|}^\infty \mathrm{d}x \; x^4 k(x, \bar{y}, \bar{z}). \tag{5.24}$$

Here, $k(x, \bar{y}, \bar{z})$ is given in (5.15). Note that $k > 0$ because $\Xi - \Psi > 0$, $\Psi > 0$ and $x \geqslant |\bar{y}|$.

The quasineutrality condition (4.60) gives the poloidally varying electric potential in the high flow limit,

$$\left(\frac{e n_e}{T_e} + \frac{Z^2 n_i e}{T} \right) \phi_c = -Z n_i \frac{r}{R} \frac{m u^2}{T}. \tag{5.25}$$

The only contribution to the potential comes from the centrifugal force as all gradients and $m(V_\parallel + u)^2/T$ terms are small while $V_\parallel \simeq -u \sim v_t$.

The low flow neoclassical results can be retrieved by taking the limit of small radial electric field, $u/v_t \ll 1$, small mean parallel flow, $V_\parallel/v_t \ll 1$, and small gradients. It follows from (5.25) that the poloidal variation of the potential is small so that we can set $\bar{z} = 0$ in the arguments of G_1, G_2, H_1, and H_2. Without a source of parallel momentum $\gamma = 0$, equation (5.6) gives $\Gamma = 0$, so the mean parallel flow follows directly from (5.20)

$$V_\parallel = -\frac{IT}{m\Omega} \left(\frac{\partial}{\partial \psi} \ln p + \frac{Ze}{T} \frac{\partial \Phi}{\partial \psi} - 1.17 \frac{\partial}{\partial \psi} \ln T \right). \tag{5.26}$$

The neoclassical energy flux Q then follows directly from (5.21) for $\Delta\bar{Q} = 0.79$ and reads

$$Q = -1.35 \sqrt{\frac{r}{R}} \frac{I^2 \nu p T}{m\Omega^2} \frac{\partial}{\partial \psi} \ln T, \tag{5.27}$$

in agreement with Hinton & Wong (1985) and Catto *et al.* (1987).

We can compare our results with those of Catto *et al.* (2013) by taking the limit of

small temperature gradient and small $V_\parallel$. We are able to retrieve the same energy flux if we set $\phi_\theta = 0$, $\Gamma = 0$ and correct an error in Catto *et al.* (2011) and pointed out by Shaing & Hsu (2012). The calculation is presented in detail in Appendix G.1.

The energy flux Q in (5.16) is proportional to $|S|^{-3/2}$ and decays $\sim \exp\left(-\bar{y}^2\right)$ which is consistent with the results of strong radial electric field and radial electric field shear obtained by Shaing & Hazeltine (1992); Shaing & Hsu (2012). We compare our results in the limit $(I/\Omega)(\partial V_\parallel/\partial\psi) \ll 1$ and $\Gamma = 0$ to those of Shaing & Hsu (2012) in Appendix G.2. We find the same particle and energy equations if we account for a discrepancy in the function $k(x, \bar{y}, \bar{z})$.

6. Transport equations and flux conditions

We work with equations (5.6), (5.12) and (5.16) to find relations between the particle flux Γ, the parallel momentum input γ, the energy flux Q, and the physical quantities T, n, u, $V_\parallel$, and ϕ_c. Given Γ and Q as functions of ψ, and boundary conditions at the top or bottom of the transport barrier, we can integrate the equations to obtain the profiles of T, n, u, $V_\parallel$, and ϕ_c.

So far, we have an equation for the particle flux (5.12), the parallel momentum equation (5.6), the energy flux (5.16) and quasineutrality (4.60). We are missing an equation for the radial electric field to be able to relate Γ, γ and Q with T, n, u, $V_\parallel$ and ϕ_c. The equation for the radial electric field is provided by the conservation of toroidal angular momentum, but the necessary derivation is beyond the scope of this paper. For the purpose of the following calculations, we assume that for the ions, the pressure gradient is the dominant contribution in the radial force balance (McDermott *et al.* 2009; Viezzer *et al.* 2013; Kagan & Catto 2008). Hence, we impose

$$Zen\frac{\partial\Phi}{\partial\psi} + \frac{\partial p}{\partial\psi} = 0, \tag{6.1}$$

which can be written as

$$\frac{\partial}{\partial\psi}\ln n = -\frac{\Omega m u}{IT} - \frac{\partial}{\partial\psi}\ln T. \tag{6.2}$$

We introduce the new, dimensionless quantities,

$$\bar{u} = \sqrt{\frac{m}{2T_0}}u, \qquad \bar{V} = \sqrt{\frac{m}{2T_0}}V_\parallel, \qquad \bar{T} = \frac{T}{T_0}, \qquad \bar{n} = \frac{n}{n_0}, \qquad \bar{\phi}_c = \frac{Ze\phi_c R}{T_0 r} \tag{6.3}$$

$$\frac{\partial}{\partial\bar{\psi}} = \frac{I}{\Omega}\sqrt{\frac{2T_0}{m}}\frac{\partial}{\partial\psi}, \qquad \bar{z} = \bar{T}^{-1}\left(2\bar{u}^2 - \bar{\phi}_c\right), \qquad \bar{y} = \frac{\bar{u} + \bar{V}}{\sqrt{\bar{T}}}, \tag{6.4}$$

where T_0 is the ion temperature and n_0 the ion density at the boundary $\psi = 0$. In the banana regime, the normalised fluxes are

$$\bar{\Gamma} = \frac{\Gamma}{n_0 I\sqrt{\frac{2T_0 r}{mR}}\frac{\nu_0}{\Omega}}, \qquad \bar{Q} = \frac{Q}{n_0 I\sqrt{\frac{2T_0 r}{mR}}T_0\frac{\nu_0}{\Omega}}, \qquad \bar{\gamma} = \frac{\gamma}{\nu_0 n_0\sqrt{2mT_0 r/R}}, \tag{6.5}$$

where ν_0 is the collision frequency at the boundary. Changing to these dimensionless variables, we arrive at the following set of equations for the banana regime: The particle

flux equation from (5.12) and (6.2) is

$$\bar{\Gamma} = -0.55\frac{\bar{n}^2}{|S|^{3/2}\bar{T}^{3/2}}\left\{\left[-2\bar{u} - 2(\bar{u}+\bar{V})\left(\frac{\partial\bar{V}}{\partial\bar{\psi}} - 1\right)\right]G_1(\bar{y},\bar{z}) - 1.17\frac{\partial\bar{T}}{\partial\bar{\psi}}G_2(\bar{y},\bar{z})\right\}. \tag{6.6}$$

The parallel momentum equation from (5.6) is

$$\bar{u}\frac{\partial\bar{\Gamma}}{\partial\bar{\psi}} + S\bar{\Gamma} = -\bar{\gamma}. \tag{6.7}$$

The energy flux equation from (5.12), (5.16), and (6.2) is

$$\bar{Q} = \bar{u}^2\bar{\Gamma} - 0.73\frac{\bar{n}^2}{|S|^{3/2}\bar{T}^{1/2}}\left\{\left[-2\bar{u} - 2(\bar{u}+\bar{V})\left(\frac{\partial\bar{V}}{\partial\bar{\psi}} - 1\right)\right]H_1(\bar{y},\bar{z}) - 0.25\frac{\partial\bar{T}}{\partial\bar{\psi}}H_2(\bar{y},\bar{z})\right\}. \tag{6.8}$$

The pressure balance equation from (6.2) gives

$$\frac{\partial}{\partial\bar{\psi}}\ln\bar{n} = -2\frac{\bar{u}}{\bar{T}} - \frac{\partial}{\partial\bar{\psi}}\ln\bar{T}; \tag{6.9}$$

and the equation for the potential, which can be derived from (4.60), is

$$\begin{aligned}
&\left\{1 - \frac{ZT_e}{T_0}\frac{1}{\bar{T}}\left[\sqrt{\bar{T}}J\left(-2\frac{\bar{u}}{\bar{T}} - \frac{3}{2}\frac{\partial}{\partial\bar{\psi}}\ln\bar{T}\right) + \left(1 - 2\frac{\bar{V}+\bar{u}}{\sqrt{\bar{T}}}J\right)\left(\frac{\partial\bar{V}}{\partial\bar{\psi}} - 1 - \frac{\bar{V}+\bar{u}}{2}\frac{\partial}{\partial\bar{\psi}}\ln T\right)\right]\right\}\bar{z} \\
&= \frac{ZT_e}{T_0}\frac{1}{\bar{T}}\left\{\sqrt{\bar{T}}J\left[\left(2\frac{\bar{V}^2 - \bar{u}^2}{\bar{T}} + 1\right)\left(-2\frac{\bar{u}}{\bar{T}} - \frac{3}{2}\frac{\partial}{\partial\bar{\psi}}\ln\bar{T}\right) + \frac{\partial}{\partial\bar{\psi}}\ln\bar{T}\right]\right. \\
&+ \left[1 - 2\frac{\bar{V}+\bar{u}}{\sqrt{\bar{T}}}J\right]\left[(\bar{V}-\bar{u})\left(-2\frac{\bar{u}}{\bar{T}} - \frac{3}{2}\frac{\partial}{\partial\bar{\psi}}\ln\bar{T}\right)\right. \\
&+ \left(\frac{\partial\bar{V}}{\partial\bar{\psi}} - 1\right)\left(1 - 2\frac{(\bar{V}+\bar{u})^2}{\bar{T}}\right) - (\bar{V}+\bar{u})\left(\frac{\bar{V}^2 - \bar{u}^2}{\bar{T}} + \frac{1}{2}\right)\frac{\partial}{\partial\bar{\psi}}\ln\bar{T}\Big] \\
&\left.+ \left[1 + 2\frac{(\bar{V}+\bar{u})^2}{\bar{T}} - 4\frac{(\bar{V}+\bar{u})^3}{\bar{T}^{3/2}}J\right]\left(\frac{\partial\bar{V}}{\partial\bar{\psi}} - 1 + \frac{\bar{V}-\bar{u}}{2}\frac{\partial}{\partial\bar{\psi}}\ln\bar{T}\right) + 2 + 2\frac{T_0}{ZT_e}\bar{u}^2\right\}.
\end{aligned} \tag{6.10}$$

The functions J, G_1, G_2, H_1, and H_2 are given in (4.58), (5.13), (5.14), (5.17), and (5.18). This set of equations is the most important result of our calculation and allow a discussion of the neoclassical transport of ions in strong gradient regions.

We can integrate equations (6.6)-(6.10) relating $\bar{n}$, $\bar{T}$, $\bar{u}$, $\bar{V}$, and $\bar{z}$ numerically by imposing boundary conditions at the top of the transport barrier and specifying particle, parallel momentum and energy sources to find profiles in the pedestal. We discuss the implications for particle (section 6.1) and energy flux (section 6.2) before presenting some example profiles (section 6.3).

6.1. *Particle flux and parallel momentum injection*

In order to understand the appearance of a neoclassical particle flux, we analyse the parallel momentum equation (6.7). In edge transport barriers, measurements of the radial electric field have shown that in the pedestal $\partial\phi/\partial\psi > 0$ and thus $\bar{u} > 0$ (McDermott

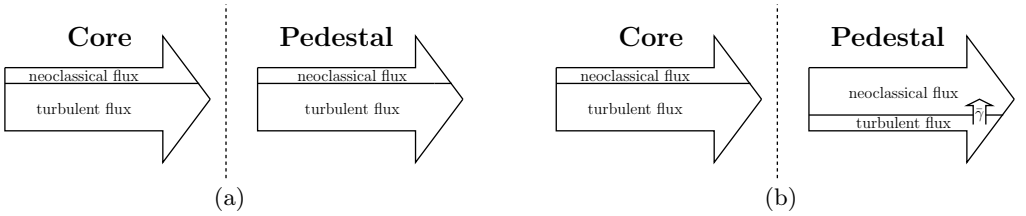

FIGURE 8. a) The entire particle flux is carried by turbulence and the neoclassical particle flux stays negligible. b) Turbulence interact with neoclassical physics and supplies a parallel momentum source that allows a growing neoclassical particle flux.

et al. 2009). We assumed that in the pedestal $\bar{u} \sim 1$. However, at the boundary to the large turbulent transport region, where our model connects to the usual neoclassical regime of small gradients in density and temperature, $\bar{u} \ll 1$. Thus, we are looking for solutions with a growing positive $\bar{u}$ as one moves into the transport barrier. Importantly, if there is no parallel momentum input, the particle flux must decay to ensure that $\bar{u}$ grows, because it follows from (6.7) that

$$\bar{\Gamma} \propto \exp\left(-\int \mathrm{d}\bar{\psi}\ \frac{S}{\bar{u}}\right). \tag{6.11}$$

For $\bar{u} > 0$ and $S > 0$, the neoclassical particle flux $\bar{\Gamma}$ decreases and is even smaller inside a transport barrier than outside when $\bar{\gamma} = 0$.

We argued in section 2 that at the inner edge of a transport barrier there is a region of large turbulent transport and small collisional transport whereas in the transport barrier, we find a region of low turbulence. In order to keep up the same total flux, the neoclassical fluxes must increase and pick up the decreasing turbulent fluxes (see figure 1). However, this initial picture is too simple as it disagrees with our analysis of the decreasing particle flux. One option to solve the contradiction is that the particle flux is still carried by turbulence because the neoclassical fluxes never pick up the turbulent contribution. There must be enough turbulence in the transport barrier to carry the entire particle flux – recall that at this point we are only discussing the particle flux and not the energy flux. So even if the entire particle flux is carried by turbulence, the energy flux could still be neoclassical (see figure 8a). The second option is that the particle flux is truly neoclassical in the transport barrier, but turbulence or impurities supply the necessary parallel momentum source γ so that (6.11) is not valid. Somehow, and we can not specify at this point how exactly, turbulence or impurities interact with neoclassical transport and appear as a source of parallel momentum (see figure 8b). The difference between the two options is that in the first picture, the neoclassical particle flux is close to zero whereas in the second picture the particle flux is in large part neoclassical because turbulence or impurities produce $\bar{\gamma}$. It is also worth pointing out that $\bar{\Gamma}$ and $\bar{\gamma}$ are necessarily of opposite sign if $\left|\bar{\Gamma}\right|$ grows as one moves into the transport barrier. An outwards neoclassical ion particle flux requires a negative parallel momentum injection.

6.2. *Energy Flux*

Next, we want to discuss the energy flux equation (6.8). In transport barriers, $\bar{T}$ and $\bar{n}$ decrease. One can use this behaviour to estimate the energy flux in this case. Combining

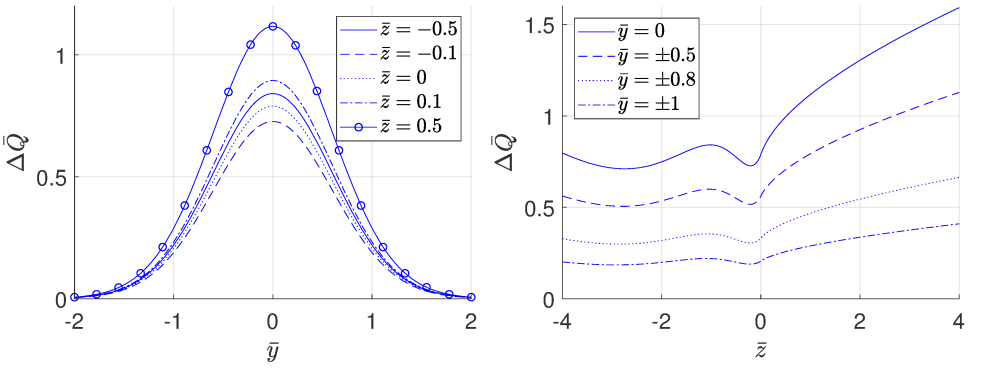

(a) (b)

FIGURE 9. (a): The quantity $\Delta\bar{Q}$ in (5.22) as a function of $\bar{y}$ for different values of $\bar{z}$. (b): The quantity $\Delta\bar{Q}$ as a function of $\bar{z}$ for different values of $\bar{y}$.

(6.6) and (6.8) to solve for $\partial\bar{T}/\partial\bar{\psi}$ as a function of $\bar{Q}$ and $\bar{\Gamma}$ yields

$$\frac{\partial\bar{T}}{\partial\bar{\psi}} = -\underbrace{1.17\frac{|S|^{3/2}\bar{T}^{1/2}}{\bar{n}^2}}_{>0}\underbrace{\frac{1}{\Delta\bar{Q}}}_{\geqslant 0}\left\{\bar{Q} - \left[\bar{u}^2 + 1.33\bar{T}\frac{H_1(\bar{y},\bar{z})}{G_1(\bar{y},\bar{z})}\right]\bar{\Gamma}\right\}, \tag{6.12}$$

where $\Delta\bar{Q}$ was defined in (5.22). Figure 9 shows $\Delta\bar{Q}$ for different values of $\bar{y}$ and $\bar{z}$. It is large for small $\bar{y}$, symmetric in $\bar{y}$ with a maximum at $\bar{y} = 0$, and asymmetric in $\bar{z}$ with larger values for $\bar{z} > 0$. When $\bar{z}$ increases so does the number of trapped particles. Thus, $\Delta\bar{Q}$ is large when there are many trapped particles.

In order to get a negative temperature gradient, the expression in braces in (6.12) must be positive. Thus, we find a lower bound for the energy flux

$$\bar{Q} \geqslant \bar{Q}_{\min} = \left[\bar{u}^2 + 1.33\bar{T}\frac{H_1(\bar{y},\bar{z})}{G_1(\bar{y},\bar{z})}\right]\bar{\Gamma}. \tag{6.13}$$

The factor multiplying $\bar{\Gamma}$ is positive because $\bar{u}^2 \geqslant 0$, $\bar{T} \geqslant 0$, and $k > 0$ and $x \geqslant |\bar{y}|$ in (5.13) and (5.17). From this, we see that it is not possible to only have neoclassical particle flux and zero neoclassical energy flux. As long as there is neoclassical particle flux, energy will get advected by that particle flux. Thus the energy flux will be in the same direction as the particle flux. The quantity $\bar{Q}_{\min}$ is shown in figure 10. It is large for large $|\bar{y}|$ and small $\bar{z}$.

Surprisingly, a negative density gradient imposes an upper boundary for $\bar{Q}$. From (6.9) it follows that for $\partial\bar{n}/\partial\bar{\psi} < 0$,

$$\frac{2\bar{n}}{\bar{T}}\bar{u} > 1.17\frac{|S|^{3/2}}{\bar{n}\bar{T}^{1/2}}\frac{\bar{Q} - \bar{Q}_{\min}}{\Delta\bar{Q}} \tag{6.14}$$

and thus we find that in order for $\bar{T}$ and $\bar{n}$ to decay simultaneously, the neoclassical energy flux has to be

$$\bar{Q}_{\min} < \bar{Q} < \bar{Q}_{\min} + 1.71\frac{\bar{n}^2\bar{u}}{\bar{T}^{1/2}|S|^{3/2}}\Delta\bar{Q}. \tag{6.15}$$

For zero neoclassical particle flux, the maximum energy flux for decaying density and

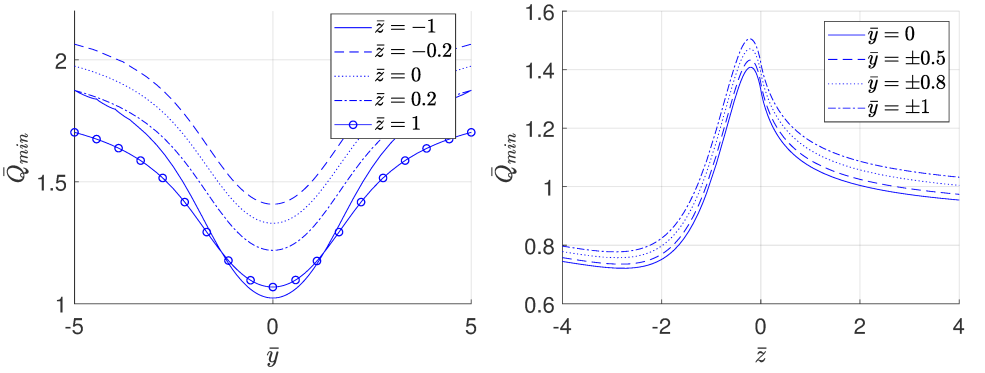

(a) (b)

FIGURE 10. (a): The quantity $\bar{Q}_{\min}$ defined in (6.13) as a function of $\bar{y}$ for different values of $\bar{z}$, where $\bar{u} = 0$, $\bar{T} = 1$ and $\bar{\Gamma} = 1$ (b): The quantity $\bar{Q}_{\min}$ as a function of $\bar{z}$ for different values of $\bar{y}$, where $\bar{u} = 0$, $\bar{T} = 1$ and $\bar{\Gamma} = 1$.

temperature profiles is

$$\bar{Q}_{\max} = 1.71 \frac{\bar{n}^2 \bar{u}}{\bar{T}^{1/2} |S|^{3/2}} \Delta\bar{Q}. \tag{6.16}$$

If the density falls off faster than the temperature in such a way that $\bar{n}^2/\sqrt{\bar{T}} \to 0$, which can be expressed as

$$L_{\bar{n}} < 4 L_{\bar{T}}, \tag{6.17}$$

then the upper bound of the energy flux in (6.15) also decreases unless it is compensated by a stronger growth in $\bar{u}\Delta\bar{Q}/|S|^{3/2}$. In most H-mode pedestals, (6.17) is observed (Viezzer *et al.* 2018, 2016). It follows, that in order to achieve a growing neoclassical energy flux, it is necessary that $\bar{u}\Delta\bar{Q}/|S|^{3/2}$ increases. Thus, the radial electric field seems to play an important role for the neoclassical energy flux at the top of transport barriers. Note, however, that the result in (6.15) relies strongly on the assumption made in (6.1) between the pressure gradient and the electric field. A more thorough discussion of this relation will be necessary and we leave it for future work. For now, using (6.2), the estimate (6.15) holds. We already argued in section 6.1 that $\bar{u}$ is positive and growing at the transition from core to pedestal. The quantity $\Delta\bar{Q}$ is large for large $|\bar{z}|$ and small $\bar{y}$ (see figure 9). This is consistent because large $|\bar{z}|$ leads to an increased number of trapped particles. Transport is dominated by trapped particles, so more trapped particles allow for a larger energy flux. Small $\bar{y}$ likewise maximises the number of trapped particles because the trapped region is located close to the maximum of the lowest order Maxwellian.

In I-mode pedestals, the temperature falls off much faster than the density (Walk *et al.* 2014). In this case, (6.17) would not necessarily hold and the neoclassical heat flux could grow with a weaker radial electric field than in H-mode.

6.3. *Example Profiles*

To show some example solutions of (6.6)-(6.10), we can take profiles of ion and electron temperature and density loosely based on those measured by Viezzer *et al.* (2016). With these profiles, we calculate fluxes, velocities and electric potential.

The integration of the mean parallel flow turns out to be very sensitive to the boundary conditions and source terms. Thus, we leave the discussion of the mean parallel flow

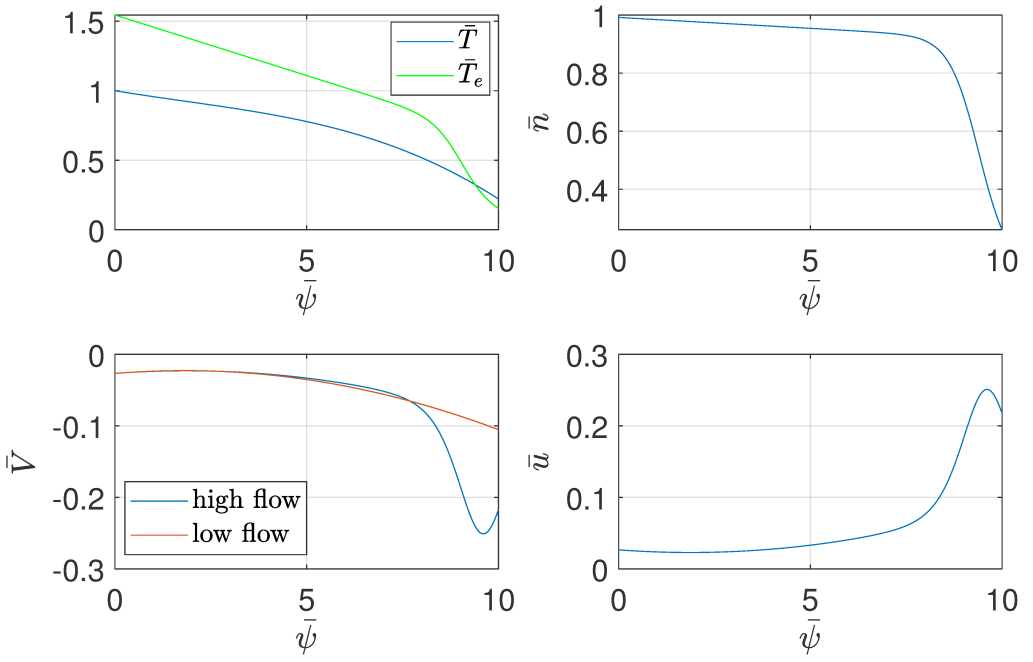

FIGURE 11. Input profiles of ion temperature, electron temperature $\bar{T}_e = T_e/T_0$, and density based on the profiles reported by Viezzer *et al.* (2016), as well as the corresponding $\bar{u}$ and $\bar{V}$. The red profile for $\bar{V}$ is the usual neoclassical result for the mean parallel velocity as given by (5.26) and the blue curve is the "high flow" profile as given by (6.18).

solutions for future work, and instead only consider cases of known mean parallel flow. The two profiles we discuss for $\bar{V}$ are the "high flow" case and the "low flow" case. Here, "high flow" and "low flow" only refers to the relationship between the mean parallel flow and the gradients of the density, temperature and potential and not to the usual stricter limits that we have discussed at the end of section 5.

For the "high flow" profile, we set

$$\bar{V} = -\bar{u}. \tag{6.18}$$

In this case, there is no friction between trapped and passing particles and the particle flux due to a shift in the Maxwellian is small because f_M is centered around the trapped particle region (see discussion below (5.15)). For the "low flow" profile, we replace condition (6.18) with the usual neoclassical solution (5.26).

The profile of $\bar{u}$ follows directly from assumption (6.9) and consequently $\bar{V}$ is given by (6.18) for the first case or (5.26) for the second case. The quantities $\bar{T}$, $\bar{n}$, $\bar{V}$, and $\bar{u}$ based on realistic profiles or assumptions are presented in figure 11. The input profiles are further discussed in Appendix H.

The graphs in figure 11 and figure 12 show the transition between core and pedestal nicely in the sense that at $\bar{\psi} = 0$, which corresponds to $\rho_{\text{pol}} = 0.8$ in Viezzer *et al.* (2016), the profiles of density and temperature are still relatively flat. We see the expected growth of $\bar{u}$ in the strong gradient region which relaxes when the gradient of $\bar{n}$ reduces again. For $\bar{V}$, we see the difference between "high flow" and standard "low flow" neoclassical theory. The solution for $\bar{V}$ from (6.18) exceeds the standard "low flow" neoclassical result

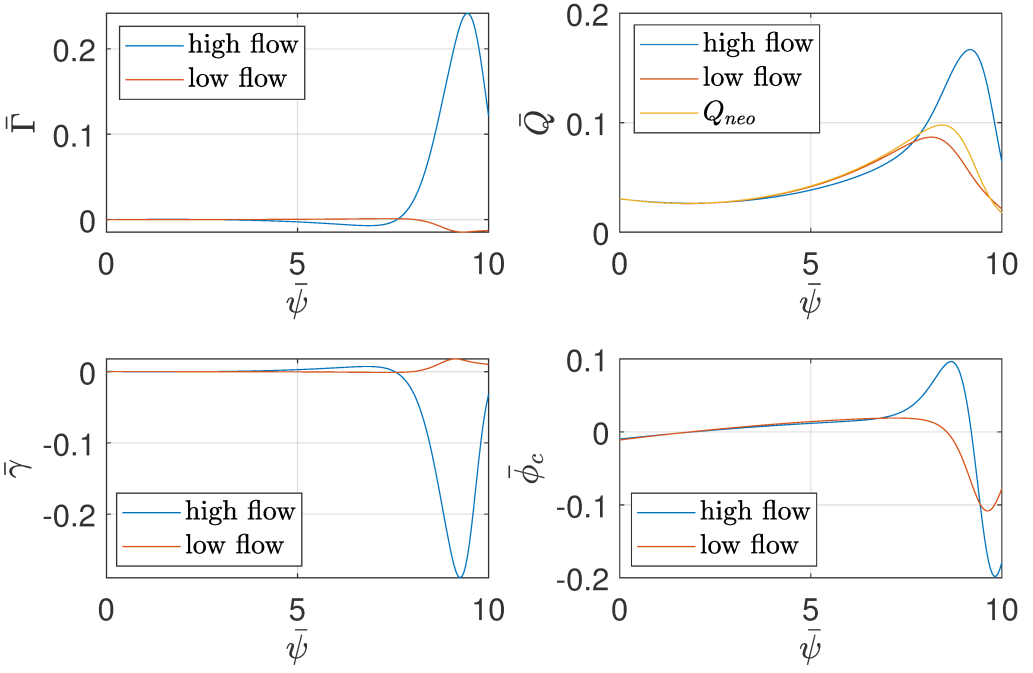

FIGURE 12. Calculated fluxes and poloidally varying potential from the profiles in figure 11. The blue profiles are the solutions with condition (6.18) whereas the red profiles show the solution with the usual neoclassical parallel velocity (5.26). The yellow energy flux is the usual neoclassical result (5.27).

in the pedestal by about a factor of two but becomes as small as the standard "low flow" neoclassical result at the boundary to the core.

Equation (6.10) gives $\bar{z}$, with which $\bar{\Gamma}$ can be calculated from (6.6). Then, the energy flux can be calculated using (6.8). Lastly, the parallel momentum input that is necessary to sustain the particle flux follows from (6.7). The four graphs for $\bar{\Gamma}$, $\bar{Q}$, $\bar{\gamma}$, and $\bar{\phi}_c$ are presented in figure 12.

The poloidally varying part of the potential is much stronger for $\bar{V} = -\bar{u}$, and changes sign in the pedestal region. The neoclassical particle flux, which is close to zero in the core requires parallel momentum input to grow. In the case with condition (6.18), the particle flux and the parallel momentum input are much bigger than for the case with the usual neoclassical parallel velocity (5.26). Note that, even for the neoclassical parallel velocity, the parallel momentum input and the particle flux are non-zero. Interestingly, the neoclassical particle flux and parallel momentum source in the pedestal for (5.26) are of opposite sign to the case with condition (6.18). The energy flux of the "high flow" case matches the standard "low flow" neoclassical result close to the inner boundary but further into the pedestal it grows faster with radius. In the case where we set the parallel velocity to be (5.26), the energy flux is smaller than the usual neoclassical result Q_{neo} of (5.27). The prefactor $\bar{n}^2/\sqrt{\bar{T}}$ in (6.8) decays in the strong gradient region for the example profiles of density and temperature, so (6.17) is satisfied, and the energy flux decays after $\bar{u}$ has reached its maximum. This is consistent with our discussion in section 6.2 and the observation that the energy transport in pedestals reaches significant neoclassical levels only in the middle of a pedestal and not at the top and bottom (Viezzer *et al.* 2020). If

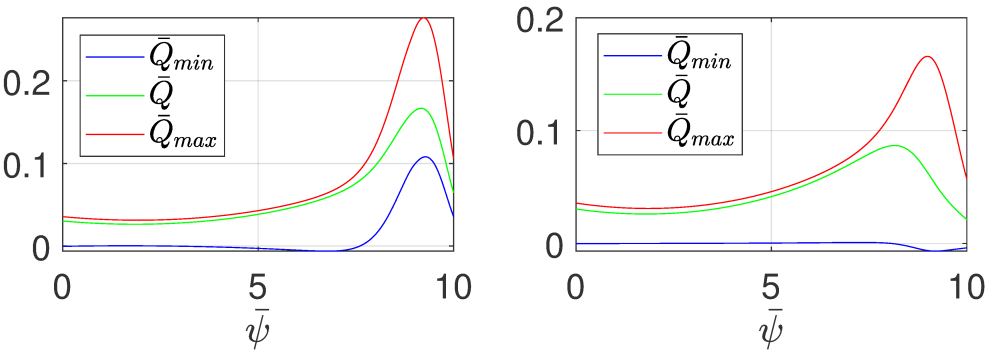

FIGURE 13. Energy flux with upper and lower bounds (6.15) in (a): the "high flow" case, and (b): the "low flow" case.

instead we had chosen profiles with a stronger temperature gradient such that $L_{\bar{n}} > 4L_{\bar{T}}$, we could have been able to retrieve a growing energy flux throughout the pedestal.

In figure 13 we show the energy fluxes and their respective lower bound (6.13) and upper bound (6.16). In both cases, the energy flux is close to the upper bound in the flat gradient region. The lower bound stays close to zero where the particle flux is small.

7. Conclusions

The core is a region of strong turbulent transport. With the transition into a transport barrier such as the pedestal, turbulence gets quenched and we argue that in order to keep up the total flux, the neoclassical fluxes must increase. This assumption is supported by experiments such as the ones by Viezzer *et al.* (2018), where it was demonstrated that the heat diffusivity reaches neoclassical levels in the pedestal. This opens the possibility of interaction between turbulent and neoclassical transport which we account for by keeping a source term that represents external particle, momentum and energy injection as well as interaction with turbulence. A random walk estimate was performed to predict the size of this source and to show that trapped particles give the main contribution to particle and energy transport.

We have extended neoclassical theory to transport barriers by choosing gradients to be of the same size as the poloidal gyroradius and expanded in large aspect ratio and low collisionality. A new set of variables, the fixed-θ variables, were derived from conserved quantities and confirmed that particles are trapped for $v_{\|} + u \sim \sqrt{\epsilon} v_t$.

A change of variables to fixed-θ variables allowed for a convenient reduction of the drift kinetic equation, to which a Maxwellian is the solution to lowest order. We have discussed the trapped-barely-passing and freely passing regions in the banana regime. The drift kinetic equation can be solved for the trapped, barely-passing, and freely passing regions by expanding in $\sqrt{\epsilon}$. The phase space region of trapped and barely-passing particles is very narrow for large aspect ratio tokamaks and can be treated as a discontinuity in the freely passing region. The only information needed from the trapped-barely-passing region is the jump (4.41) and derivative discontinuity condition (4.48). Additionally, one can find expressions for the poloidal variations of density (4.57) and potential (4.60) which have been observed previously (Theiler *et al.* 2014; Churchill *et al.* 2015; Cruz-Zabala *et al.* 2022). Particles can get trapped on the high field side because the poloidally varying part of the potential can oppose the magnetic mirror and centrifugal forces. When

integrating over velocity space, it is necessary to keep track of particles trapped on either side.

One can take moments of the freely passing particle equation (4.52) using the jump and derivative discontinuity condition to find the particle, parallel momentum and energy conservation equations (5.1), (5.5) and (5.7). From these equations, one can identify the neoclassical particle flux (5.4) and neoclassical energy flux (5.10). We find that the poloidally varying potential affects neoclassical fluxes and that the transport is dominated by trapped particles, which have a parallel velocity close to $-u$. The fluxes match with the usual neoclassical results in the appropriate limits. They equally match with the results for strong density and electric potential gradients derived by Catto *et al.* (2011) after we account for the missing orbit squeezing factor in the energy flux calculation, which was previously pointed out by Shaing & Hsu (2012). In the limit of small mean velocity gradient and zero poloidal potential, we identify a previously noted discrepancy with Shaing & Hsu (2012), but are otherwise able to reproduce their results.

The parallel momentum equation proves that a parallel momentum source is required to get a non-zero neoclassical particle flux. When there is no external parallel momentum source or sink in the edge (such as impurities or neutral beam injection), this implies that either turbulence does not decay and carries the particle flux throughout the transport barrier or that there is a mechanism by which turbulence supplies parallel momentum to neoclassical transport and the particle flux is indeed partially neoclassical.

For the energy flux, we provided upper and lower bounds in relation to the particle flux to ensure decaying profiles of temperature and density (see (6.15)). The maximum energy flux can be achieved for $\bar{V} + \bar{u} = 0$ and large $\bar{z}$. We also found that in pedestals a radially growing radial electric field is needed to obtain a radially growing neoclassical energy flux that substitutes the decreasing turbulent energy flux.

We compared the high flow case $\bar{V} = -\bar{u}$ to the standard low flow neoclassical mean parallel velocity (5.26) to find fluxes for the realistic profiles of temperature and density presented in figure 11, which are similar to those measured by Viezzer *et al.* (2016). We showed that for $\bar{V} = -\bar{u}$ the non-zero neoclassical particle flux, the energy flux, the mean parallel flow, and the poloidal variation exceed the usual neoclassical values in the strong gradient region. The neoclassical energy flux and especially the neoclassical particle flux are significantly smaller in the low flow case, but non-zero.

Funding

This work was supported by the U.S. Department of Energy under contract numbers DE-AC02-09CH11466 and DE-FG02-91ER-54109. The United States Government retains a non-exclusive, paid-up, irrevocable, world-wide license to publish or reproduce the published form of this manuscript, or allow others to do so, for United States Government purposes.

S. Trinczek was also supported by the German Academic Scholarship Foundation.

Appendix A. Orbits

A.1. *Freely passing particles*

For freely passing particles, we assume that $v_\parallel - v_{\parallel f} \sim \epsilon v_t$ and $\psi - \psi_f \sim \epsilon \rho_p R B_p$. The calculation that follows will prove these estimates correct. Subtracting the right hand

side of (3.3) from the left hand side yields

$$v_{\parallel f}(v_\parallel - v_{\parallel f}) + \mu(B - B_f) + \frac{Ze}{m}\left[(\psi - \psi_f)\frac{\partial\phi}{\partial\psi}\bigg|_{\psi_f} + (\phi_\theta - \phi_{\theta f})\right] = 0, \tag{A 1}$$

and rearranging (3.4) gives

$$\psi - \psi_f = \frac{I}{\Omega_f}(v_\parallel - v_{\parallel f}) - \frac{I}{\Omega_f}v_{\parallel f}\left(\frac{B}{B_f} - 1\right), \tag{A 2}$$

where I depends slowly on ψ and hence can be considered a function of ψ_f. Equations (A 1) and (A 2) can be combined to solve for $v_\parallel - v_{\parallel f}$ and $\psi - \psi_f$. Using the definition for u in (3.9), the deviations of parallel velocity and canonical angular momentum within the trajectory of one passing particle are

$$v_\parallel - v_{\parallel f} \simeq -\frac{(\mu B_f - v_{\parallel f}u_f)\,(B/B_f - 1) + Ze\,(\phi_\theta - \phi_{\theta f})\,/m}{v_{\parallel f} + u_f} \sim \epsilon v_t \tag{A 3}$$

and

$$\psi - \psi_f \simeq -\frac{I}{\Omega_f}\frac{(\mu B_f + v_{\parallel f}^2)\,(B/B_f - 1) + Ze(\phi_\theta - \phi_{\theta f})/m}{v_{\parallel f} + u_f} \sim \epsilon\rho_p R B_p. \tag{A 4}$$

The deviations of parallel velocity and flux function from their values at θ_f are of $O(\epsilon)$ and hence consistent with our initial assumption. We can invert expressions (A 3) and (A 4) to obtain $v_{\parallel f}$ and ψ_f from the particle coordinates at any given θ by interchanging the fixed-θ and particle variables,

$$v_{\parallel f} - v_\parallel \simeq -\frac{(\mu B - v_\parallel u)\,(B_f/B - 1) + Ze\,(\phi_{\theta f} - \phi_\theta)\,/m}{v_\parallel + u} \sim \epsilon v_t, \tag{A 5}$$

$$\psi_f - \psi \simeq -\frac{I}{\Omega}\frac{(\mu B + v_\parallel^2)\,(B_f/B - 1) + Ze(\phi_{\theta f} - \phi_\theta)/m}{v_\parallel + u} \sim \epsilon\rho_p R B_p. \tag{A 6}$$

A.2. *Trapped-barely-passing particles*

The deviations of $v_\parallel$ and ψ from $v_{\parallel f}$ and ψ_f are larger in the trapped-barely-passing region and thus the Taylor expansion of ϕ must include the second derivative in order to collect all terms to $O(\epsilon)$. We assume that $v_\parallel - v_{\parallel f} \sim \sqrt{\epsilon}v_t$ and $\psi - \psi_f \sim \sqrt{\epsilon}\rho_p R B_p$. Hence, (A 1) becomes

$$\frac{1}{2}(v_\parallel^2 - v_{\parallel f}^2) + \mu(B - B_f) + \frac{Ze}{m}\left[(\psi - \psi_f)\frac{\partial\phi}{\partial\psi}\bigg|_{\psi_f} + \frac{1}{2}(\psi - \psi_f)^2\frac{\partial^2\phi}{\partial\psi^2}\bigg|_{\psi_f} + (\phi_\theta - \phi_{\theta f})\right] = 0 \tag{A 7}$$

which, inserting (A 2), reads

$$\begin{aligned}&\frac{1}{2}(v_\parallel^2 - v_{\parallel f}^2) + (\mu B_f - v_{\parallel f}u_f)\left(\frac{B}{B_f} - 1\right) + u_f(v_\parallel - v_{\parallel f})\\ &+ \frac{1}{2}(S_f - 1)\left(v_\parallel^2 - 2v_\parallel v_{\parallel f} + v_{\parallel f}^2\right) + \frac{Ze}{m}(\phi_\theta - \phi_{\theta f}) = 0,\end{aligned} \tag{A 8}$$

where we have used the squeezing factor S_f as introduced in (3.12). Further simplifications lead to

$$\frac{1}{2}S_f\left[\left(v_\parallel - v_{\parallel f} + \frac{v_{\parallel f}+u_f}{S_f}\right)^2 - \left(v_{\parallel f} - \frac{v_{\parallel f}+u_f}{S_f}\right)^2\right] + \left(\mu B_f - v_{\parallel f}u_f\right)\left(\frac{B}{B_f}-1\right) = \frac{1}{2}(2-S_f)v_{\parallel f}^2 + u_f v_{\parallel f} - \frac{Ze}{m}\left(\phi_\theta - \phi_{\theta f}\right) \tag{A 9}$$

and finally

$$v_\parallel - v_{\parallel f} = -\frac{v_{\parallel f}+u_f}{S_f} \pm \sqrt{\frac{1}{S_f}\left[\frac{(v_{\parallel f}+u_f)^2}{S_f} - 2(\mu B_f - v_{\parallel f}u_f)\left(\frac{B}{B_f}-1\right) - 2\frac{Ze}{m}(\phi_\theta - \phi_{\theta f})\right]}. \tag{A 10}$$

It is useful to calculate $v_\parallel + u$,

$$\begin{aligned} v_\parallel + u &= (v_\parallel - v_{\parallel f}) + (u - u_f) + (v_{\parallel f} + u_f) \\ &\simeq (v_\parallel - v_{\parallel f}) + (v_{\parallel f} + u_f) + (\psi - \psi_f)\left.\frac{\partial u}{\partial \psi}\right|_{\psi_f} \\ &\simeq S_f(v_\parallel - v_{\parallel f}) + (v_{\parallel f} + u_f). \end{aligned} \tag{A 11}$$

With this result, we can write

$$v_\parallel - v_{\parallel f} = -\frac{v_{\parallel f}+u_f}{S_f} + \frac{v_\parallel + u}{S_f} \sim \sqrt{\epsilon} v_t \quad \text{and} \quad \psi - \psi_f = \frac{I}{\Omega_f}(v_\parallel - v_{\parallel f}) \sim \sqrt{\epsilon}\rho_p R B_p, \tag{A 12}$$

where

$$v_\parallel + u = \pm\sqrt{(v_{\parallel f}+u_f)^2 - 2S_f\left[(\mu B_f - u_f v_{\parallel f})\left(\frac{B}{B_f}-1\right) + \frac{Ze}{m}(\phi_\theta - \phi_{\theta f})\right]}. \tag{A 13}$$

This expression describes the trapped-barely-passing boundary and was first derived in this form by Shaing *et al.* (1994*a*). The deviations of the parallel velocity and radial position are of $O(\sqrt{\epsilon})$ and thus bigger than for passing particles, which is consistent with our initial assumption.

The solution in the trapped-barely-passing region matches with the solution in the freely passing region in the limit

$$(v_{\parallel f}+u_f)^2 \gg 2S_f\left[(\mu B_f - u_f v_{\parallel f})(B/B_f - 1) + Ze(\phi_\theta - \phi_{\theta f})/m\right], \tag{A 14}$$

since

$$v_\parallel + u \simeq (v_{\parallel f}+u_f)\left\{1 - \frac{S_f\left[(\mu B_f - u_f v_{\parallel f})(B/B_f - 1) + Ze(\phi_\theta - \phi_{\theta f})/m\right]}{(v_{\parallel f}+u_f)^2}\right\}. \tag{A 15}$$

We can invert relations (A 12) to obtain

$$v_{\parallel f} - v_\parallel = -\frac{v_\parallel + u}{S} + \frac{v_{\parallel f}+u_f}{S} \sim \sqrt{\epsilon} v_t \quad \text{and} \quad \psi_f - \psi = \frac{I}{\Omega}(v_{\parallel f} - v_\parallel) \sim \sqrt{\epsilon}\rho_p R B_p, \tag{A 16}$$

where

$$v_{\|f} + u_f = \pm\sqrt{(v_\| + u)^2 - 2S\left[(\mu B - u v_\|)\left(\frac{B_f}{B} - 1\right) + \frac{Ze}{m}(\phi_{\theta f} - \phi_\theta)\right]}. \tag{A 17}$$

Appendix B. Matching of θ-dependent parts of g_0

One can use (4.39) to prove that the θ-dependent parts of the distribution functions in the freely passing and trapped-barely-passing regime match. Following (4.39), the function g^t can be written as

$$g^t = \frac{I}{\Omega S}\left[G(\psi_f, w_f, \mu) - w\right]\mathcal{D} f_M(v_\| = -u) + \mathcal{O}(\epsilon f_M), \tag{B 1}$$

where $G - w \sim \sqrt{\epsilon} v_t$. We neglected the distinction between ψ and ψ_f in the Maxwellian and in $\mathcal{D}$ and thus terms of order ϵf_M in deriving (4.39). For barely-passing particles, (4.39) gives $G(\psi_f, w_f, \mu)$ to be

$$G(\psi_f, w_f, \mu) = G(\psi_f, w_f = 0, \mu) + \int_{w_{\mathrm{tpb}}}^{w_f} \mathrm{d}w'_f \frac{w'_f}{\langle w' \rangle_\psi}, \tag{B 2}$$

where the trapped-barely-passing boundary $w_{\mathrm{tpb}} \sim \sqrt{\epsilon} v_t$ is defined in (4.31). For trapped particles $G(\psi_f, w_f, \mu) = G(\psi_f, w_f = 0, \mu)$.

We proceed to calculate the θ-dependent piece of g^t when g^t is written as a function of ψ and w instead of ψ_f and w_f. We calculate the θ-dependent piece in the overlap region between the trapped-barely-passing and the freely passing regions. We show that g^t is independent of θ to lowest order in ϵ, and we calculate the next order θ-dependent piece, which is of order $(\epsilon v_t / w) f_M$. Note that we can calculate this small correction despite the fact that we neglect terms small in ϵ throughout the article because its size is large by a factor of $1/w$ and $\epsilon f_M \ll (\epsilon v_t / w) f_M \ll \sqrt{\epsilon} f_M$ in this region. We start by expanding (B 1) around ψ and w,

$$g^t \simeq \frac{I}{\Omega S}\left[(\psi_f - \psi)\frac{\partial G}{\partial \psi} + (w_f - w)\frac{\partial G}{\partial w} + G(\psi, w, \mu) - w\right]\mathcal{D} f_M(v_\| = -u) + \mathcal{O}(\epsilon f_M). \tag{B 3}$$

Equation (4.39) shows that, for $|w| \to \infty$, $w \simeq \langle w \rangle_\psi$ and $G(\psi_f, w_f, \mu) - w$ becomes a bounded function of order $\sqrt{\epsilon} v_t$ that only depends on ψ_f and μ. Hence, $G(\psi, w, \mu) \simeq \langle G(\psi, w, \mu) \rangle_\psi$ and the θ-dependent piece in the overlap region between the trapped-barely-passing and the freely passing regions becomes

$$\begin{aligned} g^t - \langle g^t \rangle_\psi \simeq \frac{I}{\Omega S}\Bigg[&(\psi_f - \psi - \langle \psi_f - \psi \rangle_\psi)\frac{\partial G}{\partial \psi} + (v_{\|f} - v_\| - \langle v_{\|f} - v_\| \rangle_\psi \\ &+ u_f - u - \langle u_f - u \rangle_\psi)\frac{\partial G}{\partial w}\Bigg]\mathcal{D} f_M(v_\| = -u) + \mathcal{O}(\epsilon f_M). \end{aligned} \tag{B 4}$$

We have argued above (B 4) that $G = w + \mathcal{O}(\sqrt{\epsilon} v_t)$ and thus $\partial G / \partial \psi \sim \sqrt{\epsilon} v_t / (R B_p \rho_p)$ and $\partial G / \partial w \simeq 1$. We arrive at

$$g^t - \langle g^t \rangle_\psi \simeq \frac{I}{\Omega S}\left(v_{\|f} - v_\| - \langle v_{\|f} - v_\| \rangle_\psi + u_f - u - \langle u_f - u \rangle_\psi\right)\mathcal{D} f_M(v_\| = -u) + \mathcal{O}(\epsilon v_t). \tag{B 5}$$

For $|w_f| \to \infty$ we can use (A 17) to write,

$$\begin{aligned} w_f - w &\simeq \pm\sqrt{w^2 - 2S\left[(\mu B + u^2)\left(\frac{B_f}{B} - 1\right) + \frac{Ze}{m}(\phi_{\theta f} - \phi_\theta)\right]} - w \\ &\simeq -\frac{S\left[(\mu B + u^2)\left(B_f/B - 1\right) + Ze(\phi_{\theta f} - \phi_\theta)/m\right]}{w} \end{aligned} \tag{B 6}$$

which simplifies equation (B 5) to

$$g^t - \langle g^t\rangle_\psi \xrightarrow{|w_f|\to\infty} -\frac{Ir}{\Omega R}\cos\theta\frac{u^2 + \mu B - ZeR\phi_c/(mr)}{w}\mathcal{D}f_M(v_\parallel = -u) \sim \epsilon\frac{v_t}{w}f_M. \tag{B 7}$$

Thus, $g^t - \langle g^t\rangle_\psi$ is indeed of order $\epsilon(v_t/w)f_M \gg \epsilon f_M$ and it matches with $f_{M_f} - f_M - \langle f_{M_f} - f_M\rangle_\psi$ in (4.53) for small w, as desired.

In general, for barely-passing particles one can write

$$g_0^t - \langle g_0^t\rangle_\psi = \frac{I}{\Omega S}\left(G - \langle G\rangle_\psi\right)\mathcal{D}f_M. \tag{B 8}$$

This function is odd in w since

$$G \simeq G(\psi, w_f = 0, \mu) + \int_{w_{\rm tpb}}^{w_f} \mathrm{d}w_f' \frac{w_f'}{\langle w'\rangle_\psi}, \tag{B 9}$$

giving

$$G - \langle G\rangle_\psi \simeq \int_{w_{\rm tpb}}^{w_f} \mathrm{d}w_f' \frac{w_f'}{\langle w'\rangle_\psi} - \left\langle \int_{w_{\rm tpb}}^{w_f} \mathrm{d}w_f' \frac{w_f'}{\langle w'\rangle_\psi} \right\rangle_\psi, \tag{B 10}$$

which is odd in w_f and hence in w.

Appendix C. Transit average of the collision operator

The higher order collision operator in fixed-θ variables is given in (4.42). To calculate the derivative discontinuity condition, one has to solve (4.21) and thus take the transit average of the collision operator.

We proceed to show that the transit average of (4.42) leads to equation (4.45). The drift kinetic equation in fixed-θ variables can be written as

$$\dot\theta\frac{\partial f}{\partial\theta} + \dot\psi_f\frac{\partial f}{\partial\psi_f} + \dot v_{\parallel f}\frac{\partial f}{\partial v_{\parallel f}} + \dot\mu\frac{\partial f}{\partial\mu} + \dot\varphi\frac{\partial f}{\partial\varphi} = C[f, f], \tag{C 1}$$

where the dotted quantities obey phase space conservation

$$\frac{\partial}{\partial\psi_f}\left(\mathcal{J}\dot\psi_f\right) + \frac{\partial}{\partial\theta}\left(\mathcal{J}\dot\theta\right) + \frac{\partial}{\partial v_{\parallel f}}\left(\mathcal{J}\dot v_{\parallel f}\right) + \frac{\partial}{\partial\mu}\left(\mathcal{J}\dot\mu\right) + \frac{\partial}{\partial\varphi}\left(\mathcal{J}\dot\varphi\right) = 0. \tag{C 2}$$

From the definition of ψ_f and $v_{\parallel f}$, it follows that $\dot\psi_f = 0$ and $\dot v_{\parallel f} = 0$. Furthermore, conservation of magnetic moment gives $\dot\mu = 0$. The gyrophase can be defined to higher order such that both $\dot\varphi$ and $\mathcal{J}$ are independent of gyrophase to all orders (Parra & Catto 2008). Hence, (C 2) reduces to

$$\frac{\partial}{\partial\theta}\left(\mathcal{J}\dot\theta\right) = 0. \tag{C 3}$$

We find that $\mathcal{J}\dot\theta$ is independent of θ.

Equation (C 3) can be used to take the transit average of (4.42), noting that

$$\left\langle \frac{1}{\mathcal{J}}\frac{\partial}{\partial w_f}\left[\mathcal{J}(...)\right]\right\rangle_\tau = \frac{1}{\tau}\int \frac{\mathrm{d}\theta}{\dot\theta\mathcal{J}}\frac{\partial}{\partial w_f}\left[\mathcal{J}(...)\right] = \frac{1}{\tau\dot\theta\mathcal{J}}\frac{\partial}{\partial w_f}\left[\dot\theta\mathcal{J}\int\frac{\mathrm{d}\theta}{\dot\theta}(...)\right]$$
$$= \frac{1}{\tau\dot\theta\mathcal{J}}\frac{\partial}{\partial w_f}\left[\tau\dot\theta\mathcal{J}\langle(...)\rangle_\tau\right] \simeq \frac{1}{w_f\tau}\frac{\partial}{\partial w_f}\left[w_f\tau\langle(...)\rangle_\tau\right], \tag{C 4}$$

where we used (4.43) as well as $\dot\theta \simeq w/qR$ in the last step.

Taking the transit average inside the derivatives via (C 4) and using (4.44) in (4.42) yields (4.45).

Appendix D. Integration over the distribution function

The integration of the distribution function (4.39) for the jump and derivative discontinuity condition requires the calculation of terms such as

$$\left\langle \int_{-\infty}^{\infty}\mathrm{d}w_f\frac{\partial g_0^t}{\partial w_f}\right\rangle_\psi \propto \int_{\text{barely-passing}}\mathrm{d}w_f\left(\frac{w_f}{\langle w\rangle_\psi} - \left\langle\frac{w_f}{w}\right\rangle_\psi\right) - \left\langle\int_{\text{trapped}}\mathrm{d}w_f\frac{w_f}{w}\right\rangle_\psi. \tag{D 1}$$

In (4.60) we show that $\phi_\theta = \phi_c\cos\theta$ in the banana regime, and using (3.6) and (A 13), we get

$$\frac{w}{w_f} \simeq \sqrt{1 - 2S_f(\cos\theta_f - \cos\theta)\left[(\mu B_f + u_f)^2\frac{r}{R} - \frac{Ze}{m}\phi_c\right]}. \tag{D 2}$$

For $\theta_f = 0$, this can be written as

$$\frac{w}{w_f} \simeq \sqrt{1 - \kappa^2\sin^2\left(\frac{\theta}{2}\right)} \tag{D 3}$$

where

$$\kappa^2 = \frac{r}{R}\frac{4S_f\left[\mu B_f + u_f^2 - ZeR\phi_c/(mr)\right]}{w_f^2}. \tag{D 4}$$

As a result,

$$\frac{\langle w\rangle_\psi}{w_f} = \frac{2}{\pi}E(\kappa) \tag{D 5}$$

with $E(\kappa) = \int_0^{\pi/2}\mathrm{d}\alpha\sqrt{1-\kappa^2\sin^2\alpha}$ the elliptic integral of the second kind. With these definitions, trapped particles are characterized by $1 < \kappa < \infty$, and barely-passing particles are defined by $0 < \kappa < 1$, which is in agreement with (3.13). Thus the integration in (D 1) over the barely passing region is from 0 to 1 and over the trapped region is from 1 to ∞. However, this calculation only holds for $\kappa^2 > 0$, which is not always true. In fact, $\kappa^2 > 0$ does not capture all trapped particles but only particles that are trapped on the low field side for $S_f > 0$. If ϕ_c is strong enough, it can overcome the centrifugal force and accumulate particles on the inboard side. Particles trapped on the high field side will only exist for $\phi_c > mu_f^2 r/(ZeR)$. For $S_f < 0$, these particles are captured in our definition for κ^2 in (D 4). If we set $v_{\parallel f}$ and ψ_f to be the particle velocity and position at

$\theta_f = 0$, trapped particles on the high field side that satisfy

$$\mu < \frac{Ze\phi_c R}{mB_f r} - \frac{u_f^2}{B_f} \tag{D 6}$$

for $S_f > 0$, as well as trapped particles trapped on the low field side for $S_f < 0$ are being missed out. For these particles, κ^2 in (D 4) would go negative. Thus, one must also consider the choice $\theta_f = \pi$, for which (D 3) turns into

$$\frac{w}{w_f} \simeq \sqrt{1 - \kappa^2 \cos^2\left(\frac{\theta}{2}\right)}, \tag{D 7}$$

and κ^2 is defined as

$$\kappa^2 = \frac{r}{R}\frac{4S_f\left[ZeR\phi_c/(mr) - (\mu B_f + u_f^2)\right]}{w_f^2}. \tag{D 8}$$

Using the substitution $\alpha = \pi/2 - \theta/2$ in (D 7), one arrives at the same expression for $\langle w\rangle_\psi / w_f$ as in (D 5) but with κ^2 as defined in (D 8).

D.1. *Jump Condition*

The integration for the particles that are trapped on the low (high) field side for $S_f > 0$ ($S_f < 0$) yields

$$\left\langle \int_{\text{trapped}} \mathrm{d}w_f \frac{w_f}{w} \right\rangle_\psi = \langle 2|w|\rangle_\psi\Big|_{\kappa=1} = \frac{8}{\pi}\sqrt{S_f\left[(\mu B_f + u^2)\frac{r}{R} - \frac{Ze}{m}\phi_c\right]}, \tag{D 9}$$

where the factor of 2 comes from including both possible signs of w. For the integration over the barely-passing region, we make a change of variables from w_f to κ using that

$$\frac{\mathrm{d}\kappa}{\mathrm{d}w_f} = \pm\frac{\sqrt{4S_f\left[(\mu B_f + u_f^2)r/R - Ze\phi_c/m\right]}}{w_f^2} = \pm\frac{\kappa^2}{\sqrt{4S_f\left[(\mu B_f + u_f^2)r/R - Ze\phi_c/m\right]}} \tag{D 10}$$

so that the integral can be written as

$$\begin{aligned}&\int_{\text{barely-passing}} \mathrm{d}w_f \left(\frac{w_f}{\langle w\rangle_\psi} - \left\langle\frac{w_f}{w}\right\rangle_\psi\right)\\ &= 4\sqrt{S_f\left[(\mu B_f + u_f^2)\frac{r}{R} - \frac{Ze}{m}\phi_c\right]}\int_0^1 \frac{\mathrm{d}\kappa}{\kappa^2}\left(\frac{\pi}{2E(\kappa)} - \frac{2}{\pi}K(\kappa)\right)\end{aligned} \tag{D 11}$$

with the elliptic function of the first kind.

$$K(\kappa) = \int_0^{\pi/2} \frac{\mathrm{d}\alpha}{\sqrt{1 - \kappa^2 \sin^2\alpha}}. \tag{D 12}$$

Again, one factor of two comes from keeping track of both signs of w. For particles obeying relation (D 6), the same calculations can be carried out and combining the two results (D 9) and (D 11) for particles trapped on either side and S_f of either sign yields

$$\left\langle \int_{-\infty}^{\infty} \mathrm{d}w_f \frac{\partial g_0^t}{\partial w_f} \right\rangle_\psi = -2.758\frac{I}{S\Omega}\sqrt{\left|S\left[(\mu B + u^2)\frac{r}{R} - \frac{Ze}{m}\phi_c\right]\right|}\mathcal{D}f_M(v_\parallel = -u). \tag{D 13}$$

We note that the magnetic field B_f is different at $\theta_f = 0$ and $\theta_f = \pi$, but the difference is small in ϵ as shown in section 3. At this point, we have dropped the subscript f because the difference is small in epsilon.

D.2. *Derivative discontinuity condition*

In order to calculate the derivative discontinuity condition, one has to calculate integrals of the form

$$\int_{-\infty}^{\infty} \mathrm{d}w_f \; w_f \tau \left\langle \frac{w}{w_f} \frac{\partial g_0^t}{\partial w_f} \right\rangle_\tau \tag{D 14}$$

and

$$\int_{-\infty}^{\infty} \mathrm{d}w_f \; w_f \tau \left\langle \left(\frac{w}{w_f} - 1 \right) \frac{w}{w_f} \frac{\partial g_0^t}{\partial w_f} \right\rangle_\tau \tag{D 15}$$

For barely-passing particles, (4.33) is applicable, so

$$\left\langle \frac{w^2}{w_f^2} \frac{\partial g_0^t}{\partial w_f} \right\rangle_\tau = \frac{2\pi q R}{\tau w_f} \left\langle \frac{I}{\Omega S} \left(\frac{w}{\langle w \rangle_\psi} - 1 \right) \mathcal{D} f_M(v_\parallel = -u) \right\rangle_\psi = 0, \tag{D 16}$$

and

$$\int_{\text{barely-passing}} \mathrm{d}w_f \; w_f \tau \left\langle \frac{w}{w_f} \frac{\partial g_0^t}{\partial w_f} \right\rangle_\tau = \int_{\text{barely-passing}} \mathrm{d}w_f \; 2\pi q R \left\langle \frac{\partial g_0^t}{\partial w_f} \right\rangle_\psi . \tag{D 17}$$

This integral was calculated in (D 11).

For trapped particles,

$$\left\langle \frac{w^2}{w_f^2} \frac{\partial g_0^t}{\partial w_f} \right\rangle_\tau = 0 \tag{D 18}$$

because $\partial g_0^t / \partial w_f$ is odd in w and it follows from (4.6) that transit averages over functions that are odd in w are zero for trapped particles. The remaining term is

$$\int_{\text{trapped}} \mathrm{d}w_f \; w_f \tau \left\langle \frac{w}{w_f} \frac{\partial g_0^t}{\partial w_f} \right\rangle_\tau = \left\langle \int_{\text{trapped}} \mathrm{d}w_f \; 2\pi q R \frac{\partial g_0^t}{\partial w_f} \right\rangle_\psi . \tag{D 19}$$

This integral was calculated in (D 9). Summing the contributions from barely-passing particles (D 17) and trapped particles (D 19), we arrive at the expression for the derivative discontinuity condition in (4.49).

Appendix E. Poloidal variation of the density

The poloidal variation of the density follow from the θ-dependent part of g^p. In order to find the poloidally varying part of the density in (4.54), we need to calculate the integral

$$\begin{aligned}
&\int \mathrm{d}\mu \left[\mathrm{PV}\int \mathrm{d}v_\parallel\ 2\pi B(g^p - \langle g^p\rangle_\psi)\right] \\
&= -2\pi B\int \mathrm{d}\mu\Bigg\{\mathrm{PV}\int \mathrm{d}v_\parallel \frac{Ir}{\Omega R}\frac{\left(v_\parallel^2+\mu B\right)\cos\theta - ZeR\phi_\theta/(mr)}{v_\parallel+u}\left[\frac{\partial}{\partial\psi}\ln p\right. \\
&+ \frac{m(v_\parallel - V_\parallel)}{T}\left(\frac{\partial V_\parallel}{\partial\psi} - \frac{\Omega}{I}\right) + \left(\frac{m(v_\parallel-V_\parallel)^2}{2T} + \frac{m\mu B}{T} - \frac{5}{2}\right)\frac{\partial}{\partial\psi}\ln T\Bigg] f_M \\
&\left. - \frac{r}{R}\cos\theta\frac{m}{T}\left[v_\parallel(v_\parallel - V_\parallel) + \mu B\right] f_M\right\}.
\end{aligned} \tag{E 1}$$

To calculate this integral, we first define

$$\mathcal{I} = \mathrm{PV}\int \mathrm{d}v_\parallel \frac{f_M}{v_\parallel + u} = \mathrm{PV}\int \mathrm{d}\xi \frac{f_M}{\xi + y}, \tag{E 2}$$

where $\xi \equiv v_\parallel - V_\parallel$ and $y \equiv u + V_\parallel$. The first derivative of $\mathcal{I}$ with respect to y is

$$\begin{aligned}
\frac{\partial\mathcal{I}}{\partial y} &= -\mathrm{PV}\int \mathrm{d}\xi \frac{f_M}{(\xi+y)^2} = \mathrm{PV}\int \mathrm{d}\xi \frac{\partial}{\partial\xi}\left(\frac{1}{\xi+y}\right) f_M \\
&= \mathrm{PV}\int \mathrm{d}\xi \frac{\xi}{\xi+y}\frac{m}{T} f_M = \frac{m}{T}\int \mathrm{d}\xi f_M - \mathrm{PV}\int \mathrm{d}\xi \frac{y}{\xi+y}\frac{m}{T} f_M \\
&= \frac{n}{2\pi}\left(\frac{m}{T}\right)^2 \exp\left(-\frac{m\mu B}{T}\right) - \frac{m}{T} y\mathcal{I},
\end{aligned} \tag{E 3}$$

which gives

$$\frac{\partial}{\partial y}\left[\mathcal{I}\exp\left(\frac{my^2}{2T}\right)\right] = \frac{n}{2\pi}\left(\frac{m}{T}\right)^2 \exp\left(-\frac{m\mu B}{T}\right)\exp\left(\frac{my^2}{2T}\right). \tag{E 4}$$

For $y = 0$,

$$\mathcal{I}(y=0) = \mathrm{PV}\int \mathrm{d}\xi \frac{f_M}{\xi} = 0, \tag{E 5}$$

which can be used as a boundary condition. Thus, the solution for $\mathcal{I}$ is

$$\begin{aligned}
\mathcal{I} =& \frac{n}{2\pi}\left(\frac{m}{T}\right)^2 \exp\left(-\frac{m\mu B}{T}\right)\exp\left(-\frac{my^2}{2T}\right)\int_0^y \mathrm{d}t \exp\left(\frac{mt^2}{2T}\right) \\
\equiv& \frac{2n}{\pi}\left(\frac{m}{2T}\right)^{3/2}\exp\left(-\frac{m\mu B}{T}\right) J,
\end{aligned} \tag{E 6}$$

where J is given in (4.58).

Furthermore, we find that

$$\mathrm{PV}\int \mathrm{d}\xi \frac{\xi}{\xi+y} f_M = \int \mathrm{d}\xi\ f_M - (V_\parallel + u)\mathcal{I} = \frac{n}{2\pi}\frac{m}{T}\exp\left(-\frac{m\mu B}{T}\right) - (V_\parallel+u)\mathcal{I} \tag{E 7}$$

$$\mathrm{PV}\int \mathrm{d}\xi \frac{\xi^2}{\xi+y} f_M = -(V_\parallel+u)\frac{n}{2\pi}\frac{m}{T}\exp\left(-\frac{m\mu B}{T}\right) + (V_\parallel+u)^2\mathcal{I} \tag{E 8}$$

$$\mathrm{PV}\int \mathrm{d}\xi \frac{\xi^3}{\xi+y} f_M = \frac{n}{2\pi}\exp\left(-\frac{m\mu B}{T}\right)\left[1+(V_\parallel+u)^2\frac{m}{T}\right] - (V_\parallel+u)^3\mathcal{I} \tag{E 9}$$

$$\mathrm{PV}\int \mathrm{d}\xi \frac{\xi^4}{\xi+y} f_M = -(V_\parallel+u)\frac{n}{2\pi}\exp\left(-\frac{m\mu B}{T}\right)\left[1+(V_\parallel+u)^2\frac{m}{T}\right] + (V_\parallel+u)^4\mathcal{I}. \tag{E 10}$$

Expressions (E 6)-(E 10) can be used to calculate n_θ in (4.57).

Appendix F. Derivation of transport equations

In this section we show the derivation of the moment equations (5.1), (5.5) and (5.7) in more detail. A conventional moment approach (Parra & Catto 2008) is not useful when $u \sim v_t$ and $|S-1| \sim 1$, as radial scale lengths must be of order of the poloidal ion gyroradius.

F.1. *Particle Conservation*

For particle conservation, one can start by integrating (4.52) over velocity space

$$\int \mathrm{d}^3v_f \langle C_p^{(l)}[g]\rangle_\tau - \int_{V_{\mathrm{tbp}}} \mathrm{d}^3v_f \lambda \left\langle \boldsymbol{\nabla}_v \cdot \left[f_M \int \mathrm{d}^3v' f'_M \boldsymbol{\nabla}_\omega \boldsymbol{\nabla}_\omega \omega \cdot \boldsymbol{\nabla}_{v'} \left(\frac{g_0^{t'}}{f'_M}\right)\right]\right\rangle_\tau = -\int \mathrm{d}^3v_f \langle \Sigma\rangle_\tau, \tag{F 1}$$

where the passing collision operator of (4.51) in the fixed-θ variables is

$$\begin{aligned}
\langle C_p^{(l)}[g]\rangle_\tau \simeq{}& \frac{1}{w_f\tau}\frac{\partial}{\partial w_f}\left[f_M w_f \tau \left\langle \frac{w}{w_f}\hat{\boldsymbol{b}}\cdot\boldsymbol{M}\cdot\boldsymbol{\nabla}_v\left(\frac{g^p}{f_M}\right)\right\rangle_\tau\right] \\
&+ \frac{1}{w_f\tau}\frac{\partial}{\partial \mu}\left[f_M w_f \tau \left\langle \frac{\boldsymbol{v}_\perp}{B}\cdot\boldsymbol{M}\cdot\boldsymbol{\nabla}_v\left(\frac{g^p}{f_M}\right)\right\rangle_\tau\right] \\
&+ \frac{1}{w_f\tau}\frac{\partial}{\partial \psi_f}\left[f_M w_f \tau \frac{I}{\Omega S}\left\langle \left(\frac{w}{w_f}-1\right)\hat{\boldsymbol{b}}\cdot\boldsymbol{M}\cdot\boldsymbol{\nabla}_v\left(\frac{g^p}{f_M}\right)\right\rangle_\tau\right] \\
&- \lambda\left\{ \left\langle \frac{1}{w_f\tau}\frac{\partial}{\partial w_f}\left[f_M w_f\tau \frac{w}{w_f}\hat{\boldsymbol{b}}\cdot\int \mathrm{d}^3v' f'_M \boldsymbol{\nabla}_\omega\boldsymbol{\nabla}_\omega\omega\cdot\boldsymbol{\nabla}_{v'}\left(\frac{g^{p'}}{f'_M}\right)\right]\right\rangle_\tau \right. \\
&+ \left\langle \frac{1}{w_f\tau}\frac{\partial}{\partial \mu}\left[f_M w_f\tau \frac{\boldsymbol{v}_\perp}{B}\cdot\int \mathrm{d}^3v' f'_M \boldsymbol{\nabla}_\omega\boldsymbol{\nabla}_\omega\omega\cdot\boldsymbol{\nabla}_{v'}\left(\frac{g^{p'}}{f'_M}\right)\right]\right\rangle_\tau \\
&\left. + \left\langle \frac{1}{w_f\tau}\frac{\partial}{\partial \psi_f}\left[f_M w_f\tau \frac{I}{\Omega S}\left(\frac{w}{w_f}-1\right)\hat{\boldsymbol{b}}\cdot\int \mathrm{d}^3v' f'_M \boldsymbol{\nabla}_\omega\boldsymbol{\nabla}_\omega\omega\cdot\boldsymbol{\nabla}_{v'}\left(\frac{g^{p'}}{f'_M}\right)\right]\right\rangle_\tau \right\}.
\end{aligned} \tag{F 2}$$

In the passing region, $(w/w_f - 1)$ is small in ϵ and therefore the terms including the derivatives in ψ_f are negligible. One can change from transit averages to flux surface

averages using (4.33). The simplified collision operator becomes

$$\langle C_p^{(l)}[g]\rangle_\tau = \frac{\partial}{\partial w_f}\left[f_M\left\langle \hat{\boldsymbol{b}}\cdot\boldsymbol{M}\cdot\boldsymbol{\nabla}_v\left(\frac{g^p}{f_M}\right)\right\rangle_\psi\right] + \frac{\partial}{\partial \mu}\left[f_M\left\langle \frac{\boldsymbol{v}_\perp}{B}\cdot\boldsymbol{M}\cdot\boldsymbol{\nabla}_v\left(\frac{g^p}{f_M}\right)\right\rangle_\psi\right]$$
$$-\lambda\left\{\frac{\partial}{\partial w_f}\left[f_M\left\langle \hat{\boldsymbol{b}}\cdot\int \mathrm{d}^3v' f'_M \boldsymbol{\nabla}_\omega\boldsymbol{\nabla}_\omega\omega\cdot\boldsymbol{\nabla}_{v'}\left(\frac{g^{p'}}{f'_M}\right)\right\rangle_\psi\right]\right.$$
$$\left.+\frac{\partial}{\partial \mu}\left[f_M\left\langle \frac{\boldsymbol{v}_\perp}{B}\cdot\int \mathrm{d}^3v' f'_M \boldsymbol{\nabla}_\omega\boldsymbol{\nabla}_\omega\omega\cdot\boldsymbol{\nabla}_{v'}\left(\frac{g^{p'}}{f'_M}\right)\right\rangle_\psi\right]\right\}. \tag{F 3}$$

Integrating (F 3) over velocity space gives the first term in (F 1). The integration over μ cancels the respective derivative terms in (F 3) and the integration in w_f cancels the respective derivative acting on the Maxwellian in the third term in (F 3). The only term left is

$$\int \mathrm{d}^3v_f\langle C_p^{(l)}[g]\rangle_\tau = \int \mathrm{d}\mu\int \mathrm{d}w_f 2\pi B\frac{\partial}{\partial w_f}\left[f_M\left\langle \hat{\boldsymbol{b}}\cdot\boldsymbol{M}\cdot\boldsymbol{\nabla}_v\left(\frac{g^p}{f_M}\right)\right\rangle_\psi\right], \tag{F 4}$$

where we have used that $\mathrm{d}^3v_f \simeq \mathrm{d}\mu\ \mathrm{d}w_f\ 2\pi B$. The derivative is acting on the passing particle distribution function, which has a discontinuity at $w_f = 0$. We arrive at

$$\int \mathrm{d}^3v_f\langle C_p^{(l)}[g]\rangle_\tau = -\int \mathrm{d}\mu\ 2\pi B\Delta\left[f_M\left\langle \hat{\boldsymbol{b}}\cdot\boldsymbol{M}\cdot\boldsymbol{\nabla}_v\left(\frac{g^p}{f_M}\right)\right\rangle_\psi\right], \tag{F 5}$$

where the integrand on the right hand side is given by equation (4.49). For the second term in (F 1), one can follow the same steps and write the velocity divergence in terms of the fixed-θ variables. As the derivatives are not acting on the trapped distribution function but on the Maxwellian, there is no discontinuity and the integration cancels all terms in it.

Next, the derivative discontinuity condition in (4.49) is substituted into (F 5). The integration cancels the derivative in μ and we find

$$\int \mathrm{d}\mu\ 2\pi B\frac{\partial}{\partial\psi_f}\left[\frac{I}{\Omega S}M_\parallel\Delta g^p\right] = \int \mathrm{d}^3v_f\langle\Sigma\rangle_\tau. \tag{F 6}$$

for the particle equation. With the definition of the parallel friction force in (5.2) we arrive at (5.1).

F.2. *Parallel momentum conservation*

One can follow the same procedure for the derivation of the parallel momentum and energy equations. For parallel momentum conservation, we multiply (4.52) by $mv_{\parallel f}$ and

integrate over velocity space

$$\int \mathrm{d}^3 v_f \; m v_{\|f} \langle C_p^{(l)}[g] \rangle_\tau$$
$$-\int_{V_{\mathrm{tbp}}} \mathrm{d}^3 v_f \; m v_{\|f} \lambda \left\langle \boldsymbol{\nabla}_v \cdot \left[f_M \int \mathrm{d}^3 v' f'_M \boldsymbol{\nabla}_\omega \boldsymbol{\nabla}_\omega \boldsymbol{\omega} \cdot \boldsymbol{\nabla}_{v'} \left(\frac{g_0^{t'}}{f'_M} \right) \right] \right\rangle_\tau = -\int \mathrm{d}^3 v_f m v_{\|f} \langle \Sigma \rangle_\tau . \tag{F 7}$$

For the first term, one can use the expression in (F 3). Again, the integrals over μ cancel the derivatives in μ, and the only remaining terms are

$$\int \mathrm{d}^3 v_f \; m v_{\|f} \langle C_p^{(l)}[g] \rangle_\tau = \int \mathrm{d}\mu \int \mathrm{d}w_f 2\pi B m v_{\|f} \frac{\partial}{\partial w_f} \left[f_M \left\langle \hat{\boldsymbol{b}} \cdot \boldsymbol{M} \cdot \boldsymbol{\nabla}_v \left(\frac{g^p}{f_M} \right) \right\rangle_\psi \right]$$
$$- \lambda \int \mathrm{d}\mu \int \mathrm{d}w_f 2\pi B m v_{\|f} \frac{\partial}{\partial w_f} \left[f_M \left\langle \hat{\boldsymbol{b}} \cdot \int \mathrm{d}^3 v' f'_M \boldsymbol{\nabla}_\omega \boldsymbol{\nabla}_\omega \omega \cdot \boldsymbol{\nabla}_{v'} \left(\frac{g^{p'}}{f'_M} \right) \right\rangle_\psi \right]. \tag{F 8}$$

Integrating by parts leaves us with

$$\int \mathrm{d}^3 v_f \; m v_{\|f} \langle C_p^{(l)}[g] \rangle_\tau = \int \mathrm{d}\mu \; 2\pi B m u \Delta \left[f_M \left\langle \hat{\boldsymbol{b}} \cdot \boldsymbol{M} \cdot \boldsymbol{\nabla}_v \left(\frac{g^p}{f_M} \right) \right\rangle_\psi \right]$$
$$- \int \mathrm{d}\mu \int \mathrm{d}w_f \; 2\pi B m \left[f_M \left\langle \hat{\boldsymbol{b}} \cdot \boldsymbol{M} \cdot \boldsymbol{\nabla}_v \left(\frac{g^p}{f_M} \right) \right\rangle_\psi \right] \tag{F 9}$$
$$- \lambda \int \mathrm{d}\mu \int \mathrm{d}w_f 2\pi B m \left[f_M \left\langle \hat{\boldsymbol{b}} \cdot \int \mathrm{d}^3 v' f'_M \boldsymbol{\nabla}_\omega \boldsymbol{\nabla}_\omega \omega \cdot \boldsymbol{\nabla}_{v'} \left(\frac{g^{p'}}{f'_M} \right) \right\rangle_\psi \right],$$

where we have used that $v_{\|f} \simeq -u_f \simeq -u$ in the trapped-barely-passing region. The integrand of the first integral in (F 9) is given by equation (4.49). The last two terms in (F 9) can be seen to cancel by recalling the definition of $\boldsymbol{M}$ in (4.18). The only term that we are left with is

$$\int \mathrm{d}^3 v_f \; m v_{\|f} \langle C_p^{(l)}[g] \rangle_\tau = \int \mathrm{d}\mu \; 2\pi B m u \Delta \left[f_M \left\langle \hat{\boldsymbol{b}} \cdot \boldsymbol{M} \cdot \boldsymbol{\nabla}_v \left(\frac{g^p}{f_M} \right) \right\rangle_\psi \right]. \tag{F 10}$$

Substituting the derivative discontinuity condition (4.49), we find

$$\int \mathrm{d}^3 v_f \; m v_{\|f} \langle C_p^{(l)}[g] \rangle_\tau = \int \mathrm{d}\mu \; 2\pi B m u \frac{\partial}{\partial \psi_f} \left[\frac{I}{\Omega S} M_\| \Delta g^p \right]. \tag{F 11}$$

Taking the derivative with respect to ψ_f outside of the integral and using (5.2), one arrives at

$$-\int \mathrm{d}^3 v_f \; m v_{\|f} \langle \Sigma \rangle_\tau = -\frac{\partial}{\partial \psi_f} \left(\frac{I}{\Omega} u F_\| \right) + (S-1) F_\| . \tag{F 12}$$

The second term in (F 7) can be integrated by parts to find, upon using (4.23) with $w \simeq w_f$,

$$
\begin{aligned}
&-\int \mathrm{d}^3 v_f \; m v_{\parallel f} \lambda \left\langle \boldsymbol{\nabla}_v \cdot \left[f_M \int \mathrm{d}^3 v' f'_M \boldsymbol{\nabla}_\omega \boldsymbol{\nabla}_\omega \boldsymbol{\omega} \cdot \boldsymbol{\nabla}_{v'} \left(\frac{g_0^{t'}}{f'_M} \right) \right] \right\rangle_\tau \\
&= \int \mathrm{d}\mu \int \mathrm{d}w_f \; 2\pi B m \lambda \hat{\boldsymbol{b}} \cdot \left\langle \left[f_M \int \mathrm{d}^3 v' f'_M \boldsymbol{\nabla}_\omega \boldsymbol{\nabla}_\omega \boldsymbol{\omega} \cdot \boldsymbol{\nabla}_{v'} \left(\frac{g_0^{t'}}{f'_M} \right) \right] \right\rangle_\psi \\
&\simeq 2\pi B m \int \mathrm{d}\mu \int \mathrm{d}w_f f_M M_\parallel \left\langle \frac{\partial (g_0^t / f_M)}{\partial w_f} \right\rangle_\psi = -S F_\parallel .
\end{aligned}
\tag{F 13}
$$

Combining (F 12) and (F 13) gives the parallel momentum equation in the form of (5.5).

F.3. *Energy conservation*

The energy equation requires a multiplication of (4.52) by $m v_f^2/2$ and integration over velocity space

$$
\begin{aligned}
&\int \mathrm{d}^3 v_f \; \frac{m v_f^2}{2} \langle C_p^{(l)}[g] \rangle_\tau \\
&- \int_{V_{\mathrm{tbp}}} \mathrm{d}^3 v_f \; \frac{m v_f^2}{2} \lambda \left\langle \boldsymbol{\nabla}_v \cdot \left[f_M \int \mathrm{d}^3 v' f'_M \boldsymbol{\nabla}_\omega \boldsymbol{\nabla}_\omega \boldsymbol{\omega} \cdot \boldsymbol{\nabla}_{v'} \left(\frac{g_0^{t'}}{f'_M} \right) \right] \right\rangle_\tau = - \int \mathrm{d}^3 v_f \frac{m v_f^2}{2} \langle \Sigma \rangle_\tau .
\end{aligned}
\tag{F 14}
$$

Once again we can use (F 3) for the first term in (F 14) and integrate by parts to arrive at

$$
\begin{aligned}
&\int \mathrm{d}^3 v_f \; \frac{m v_f^2}{2} \langle C_p^{(l)}[g] \rangle_\tau = - \int \mathrm{d}\mu \left(\frac{m u^2}{2} + m\mu B \right) 2\pi B \Delta \left[f_M \left\langle \hat{\boldsymbol{b}} \cdot \boldsymbol{M} \cdot \boldsymbol{\nabla}_v \left(\frac{g^p}{f_M} \right) \right\rangle_\psi \right] \\
&- \int \mathrm{d}\mu \int \mathrm{d}w_f 2\pi m B v_{\parallel f} f_M \left\langle \hat{\boldsymbol{b}} \cdot \boldsymbol{M} \cdot \boldsymbol{\nabla}_v \left(\frac{g^p}{f_M} \right) \right\rangle_\psi \\
&- \int \mathrm{d}\varphi \int \mathrm{d}\mu \int \mathrm{d}w_f m B^2 f_M \left\langle \frac{\boldsymbol{v}_\perp}{B} \cdot \boldsymbol{M} \cdot \boldsymbol{\nabla}_v \left(\frac{g^p}{f_M} \right) \right\rangle_\psi \\
&+ \lambda \int \mathrm{d}\varphi \int \mathrm{d}\mu \int \mathrm{d}w_f m B (v_{\parallel f} \hat{\boldsymbol{b}} + \boldsymbol{v}_\perp) \cdot \left[f_M \left\langle \int \mathrm{d}^3 v' \; f'_M \boldsymbol{\nabla}_\omega \boldsymbol{\nabla}_\omega \omega \cdot \boldsymbol{\nabla}_{v'} \left(\frac{g^{p'}}{f'_M} \right) \right\rangle_\psi \right] .
\end{aligned}
\tag{F 15}
$$

We kept the integration over gyrophase in the last two terms of (F 15) because they seemingly depend on gyrophase via $\boldsymbol{v}_\perp$. However, this dependence cancels, because we can use that

$$
(v_{\parallel f} \hat{\boldsymbol{b}} + \boldsymbol{v}_\perp) \cdot \boldsymbol{\nabla}_\omega \boldsymbol{\nabla}_\omega \boldsymbol{\omega} = \boldsymbol{v} \cdot \boldsymbol{\nabla}_\omega \boldsymbol{\nabla}_\omega \boldsymbol{\omega} = \boldsymbol{v}' \cdot \boldsymbol{\nabla}_\omega \boldsymbol{\nabla}_\omega \boldsymbol{\omega}
\tag{F 16}
$$

and integrate over $\mathrm{d}^3 v_f$ to get $\boldsymbol{M}$. We are left with

$$
\int \mathrm{d}^3 v_f \; \frac{m v_f^2}{2} \langle C_p^{(l)}[g] \rangle_\tau = - \int \mathrm{d}\mu \left(\frac{m u^2}{2} + m\mu B \right) 2\pi B \Delta \left[f_M \left\langle \hat{\boldsymbol{b}} \cdot \boldsymbol{M} \cdot \boldsymbol{\nabla}_v \left(\frac{g^p}{f_M} \right) \right\rangle_\psi \right] .
\tag{F 17}
$$

The derivative discontinuity condition (4.49) can be used to yield

$$\int \mathrm{d}^3 v_f \ \frac{m v_f^2}{2} \langle C_p^{(l)}[g] \rangle_\tau = \int \mathrm{d}\mu \int \mathrm{d}w_f 2\pi m B^2 \mu \frac{\partial}{\partial \mu} \left(2\mu M_\perp \Delta g^p\right) \\ - \int \mathrm{d}\mu \ 2\pi B m \frac{u^2 + 2\mu B}{2} \frac{\partial}{\partial \psi_f} \left(\frac{I}{\Omega S} M_\parallel \Delta g^p \right). \tag{F 18}$$

We can integrate by parts in the first term and take the derivative with respect to ψ_f out of the integral and find

$$\int \mathrm{d}^3 v_f \ \frac{m v_f^2}{2} \langle C_p^{(l)}[g] \rangle_\tau = - \int \mathrm{d}\mu \ 4\pi m B^2 \mu M_\perp \Delta g^p - (S-1) u F_\parallel - \frac{\partial}{\partial \psi_f} \left(\frac{I}{\Omega} \Theta \right), \tag{F 19}$$

where we introduced the heat viscous force Θ defined in (5.8).

The second term in (F 14) can be integrated by parts to give

$$- \int \mathrm{d}^3 v_f \ \frac{m v_f^2}{2} \lambda \left\langle \boldsymbol{\nabla}_v \cdot \left[f_M \int \mathrm{d}^3 v' f'_M \boldsymbol{\nabla}_\omega \boldsymbol{\nabla}_\omega \boldsymbol{\omega} \cdot \boldsymbol{\nabla}_{v'} \left(\frac{g_0^{t'}}{f'_M} \right) \right] \right\rangle_\tau \\ = \int \mathrm{d}\varphi \int \mathrm{d}\mu \int \mathrm{d}w_f B m \lambda \left(v_{\parallel f} \hat{\boldsymbol{b}} + \boldsymbol{v}_\perp \right) \cdot \left[f_M \left\langle \int \mathrm{d}^3 v' f'_M \boldsymbol{\nabla}_\omega \boldsymbol{\nabla}_\omega \boldsymbol{\omega} \cdot \boldsymbol{\nabla}_{v'} \left(\frac{g_0^{t'}}{f'_M} \right) \right\rangle_\psi \right]. \tag{F 20}$$

The integrations over $\boldsymbol{v}$ and $\boldsymbol{v}'$ can be swapped using relation (F 16), which then gives $\boldsymbol{M}$. As a result

$$\begin{aligned} &- \int \mathrm{d}^3 v_f \ \frac{m v_f^2}{2} \lambda \left\langle \boldsymbol{\nabla}_v \cdot \left[f_M \int \mathrm{d}^3 v' f'_M \boldsymbol{\nabla}_\omega \boldsymbol{\nabla}_\omega \boldsymbol{\omega} \cdot \boldsymbol{\nabla}_{v'} \left(\frac{g_0^{t'}}{f'_M} \right) \right] \right\rangle_\tau \\ &= \int \mathrm{d}\mu \int \mathrm{d}w_f \ 2\pi B m f_M \left\langle \boldsymbol{v}_f \cdot \boldsymbol{M} \cdot \boldsymbol{\nabla}_v \left(\frac{g_0^t}{f_M} \right) \right\rangle_\psi \\ &= u S F_\parallel + \int \mathrm{d}\mu \ 4\pi m B^2 \mu M_\perp \Delta g^p. \end{aligned} \tag{F 21}$$

The two terms containing $M_\perp$ cancel when substituting (F 19) and (F 21) into (F 14), which leaves us with energy equation (5.7).

Appendix G. Comparison to previous work

G.1. *Small temperature gradient limit*

Equations (5.12) and (5.16) can reproduce the results for the ion energy flux in the banana limit derived by Catto *et al.* (2013) when taking the limit of small temperature gradient, small particle flux, small mean velocity and small mean velocity gradient. To lowest order, (5.12) gives

$$\frac{\partial}{\partial \psi} \ln n + \frac{m \Omega u}{I T} = 0. \tag{G 1}$$

To next order,

$$\Gamma = -1.102 \sqrt{\frac{R}{r}} \frac{\nu I q p}{|S|^{3/2} m \Omega^2} \left[\left(\frac{\partial}{\partial \psi} \ln T - \frac{m u}{T} \frac{\partial V_\parallel}{\partial \psi} \right) G_1(\bar{y}, \bar{z}) - 1.17 \frac{1}{T} \frac{\partial T}{\partial \psi} G_2(\bar{y}, \bar{z}) \right]. \tag{G 2}$$

Similarly, the energy flux reduces to

$$Q = \frac{mu^2}{2}\Gamma - 1.463\sqrt{\frac{R}{r}}\frac{qI\nu p}{|S|^{3/2}\Omega^2}\frac{T}{m}\left[\left(\frac{\partial}{\partial\psi}\ln T - \frac{mu}{T}\frac{\partial V_\parallel}{\partial\psi}\right)H_1(\bar{y},\bar{z}) - 0.25\frac{1}{T}\frac{\partial T}{\partial\psi}H_2(\bar{y},\bar{z})\right], \quad (G\,3)$$

We can solve (G 2) for $T^{-1}(\partial T/\partial\psi) - (mu/T)(\partial V_\parallel/\partial\psi)$ and substitute this into (G 3).

$$Q = \left(\frac{mu^2}{2} + 1.33T\frac{H_1}{G_1}\right)\Gamma - 1.71\sqrt{\frac{R}{r}}\frac{qI\nu p}{|S|^{3/2}\Omega^2 m}\frac{\partial T}{\partial\psi}\Delta\bar{Q}, \quad (G\,4)$$

where $\Delta\bar{Q}$ was defined in (5.22). Furthermore, Catto *et al.* (2013) assumed $\Gamma = 0$ and no poloidally varying potential. Neglecting the poloidal potential variation is consistent with our model as it follows from (4.60) that for small temperature gradient, $V_\parallel \ll v_t$ and $\Gamma = 0$, the electric potential $\phi_c = 0$ and hence $\bar{z} = 2\bar{u}^2$, where $\bar{u} = u/v_t$. We impose these restriction on (G 4) in order to get an energy flux consistent with the energy flux of Catto, and find

$$Q = -1.71\sqrt{\frac{R}{r}}\frac{qI\nu p}{|S|^{3/2}\Omega^2 m}\Delta\bar{Q}\frac{\partial T}{\partial\psi}. \quad (G\,5)$$

The energy flux in Catto *et al.* (2013) is

$$Q = -1.35\sqrt{\frac{R}{r}}\frac{qI\nu p}{|S|^{1/2}\Omega^2 m}L(\bar{u}^2)\frac{\partial T}{\partial\psi} \quad (G\,6)$$

where

$$L = 1.53e^{-\bar{u}^2}\int_0^\infty \mathrm{d}\bar{\mu}(\bar{\mu}+2\bar{u}^2)^{3/2}(\bar{\mu}+2\bar{u}^2-\sigma)(\bar{\mu}+\bar{u}^2)^{-3/2}\{\bar{\mu}\left[\Xi(x)-\Psi(x)\right] + 2\bar{u}^2\Psi(x)\}\exp(-\bar{\mu}), \quad (G\,7)$$

$$\sigma = \frac{\int_0^\infty \mathrm{d}\bar{\mu}e^{-\bar{\mu}}(\bar{\mu}+2\bar{u}^2)^{3/2}\left[\bar{\mu}\nu_\perp(x)+2\bar{u}^2\nu_\parallel(x)\right]}{\int_0^\infty \mathrm{d}\bar{\mu}e^{-\bar{\mu}}(\bar{\mu}+2\bar{u}^2)^{1/2}\left[\bar{\mu}\nu_\perp(x)+2\bar{u}^2\nu_\parallel(x)\right]}, \quad (G\,8)$$

and $\bar{\mu} = m\mu/(BT) \simeq x^2 - \bar{u}^2$. One can write

$$\sigma = \frac{\int_{|\bar{u}|}^\infty \mathrm{d}x\ (x^2+\bar{u}^2)k(x,\bar{u})}{\int_{|\bar{u}|}^\infty \mathrm{d}x\ k(x,\bar{u})} \quad (G\,9)$$

and

$$L(\bar{u}^2) = 6.12\int_{|\bar{u}|}^\infty \mathrm{d}x\left(x^4+2x^2\bar{u}^2+\bar{u}^4-\sigma(x^2+\bar{u}^2)\right)k(x,\bar{u}) = 1.27\Delta\bar{Q}. \quad (G\,10)$$

Finally, the energy flux of Catto *et al.* (2013) is

$$Q = -1.71\sqrt{\frac{R}{r}}\frac{qI\nu p}{|S|^{1/2}\Omega^2 m}\Delta\bar{Q}\frac{\partial T}{\partial\psi}. \quad (G\,11)$$

The energy fluxes in (G 5) and (G 11) differ by a factor of $1/S$. However, when the energy flux was calculated in equation (38) in Catto *et al.* (2013) and previously in Catto *et al.* (2011), this factor had been missed as already pointed out by Shaing & Hsu (2012). The

energy flux can be obtained from the lowest order moment $Iv_f^2 w_f/B$ of the drift kinetic equation (4.2),

$$\left\langle \int d^3v_f \frac{w_f I}{B} v_f^2 \frac{w}{qR} \frac{\partial f}{\partial \theta}\bigg|_{v_{\|f},\psi_f} \right\rangle_\psi = \left\langle \int d^3v_f \frac{w_f I}{B} v_f^2 C[f,f] \right\rangle_\psi . \tag{G 12}$$

One can integrate the left hand side by parts in θ to find

$$\left\langle \int d^3v_f \frac{w_f I}{B} v_f^2 \frac{w}{qR} \frac{\partial f}{\partial \theta}\bigg|_{v_{\|f},\psi_f} \right\rangle_\psi = -\left\langle \int d^3v_f \frac{w_f I}{B} \frac{v_f^2}{qR} \frac{\partial w}{\partial \theta}\bigg|_{v_{\|f},\psi_f} f \right\rangle_\psi . \tag{G 13}$$

Using (A 13) for

$$\frac{\partial w}{\partial \theta}\bigg|_{v_{\|f},\psi_f} = -\frac{S_f}{w}\left[\left(\mu B_f + u_f^2\right)\frac{r}{R}\sin\theta + \frac{Ze}{m}\frac{\partial \phi_\theta}{\partial \theta}\right] \simeq \frac{S}{w}\frac{\Omega}{I} qR \boldsymbol{v}_d \cdot \boldsymbol{\nabla}\psi, \tag{G 14}$$

we find the squeezing factor that was lost in Catto *et al.* (2013). The collision operator conserves energy, so w_f on the right hand side can be reduced to $v_{\|f}$ and we arrive at

$$-\left\langle \frac{ZeS}{mc} \int d^3v_f \frac{w_f}{w} v_f^2 f \boldsymbol{v}_d \cdot \boldsymbol{\nabla}\psi \right\rangle_\psi = \left\langle \int d^3v_f \frac{v_{\|f} I}{B} v_f^2 C[f,f] \right\rangle_\psi . \tag{G 15}$$

The energy flux in Catto *et al.* (2013) is defined as

$$Q = \frac{IqR}{r}\left\langle \int d^3v \ \frac{mv^2}{2} f \boldsymbol{v}_d \cdot \boldsymbol{\nabla}\psi \right\rangle_\psi . \tag{G 16}$$

We can combine (G 15) and (G 16), and use that in the trapped region $d^3v \simeq d^3v_f \ w_f/w$ and that the collision operator conserves momentum to arrive at

$$Q = -\frac{1}{S}\frac{mcI^2 qRT}{Zer}\left\langle \int \frac{d^3v}{B}\left(\frac{mv^2}{2T} - \frac{5}{2}\right) v_\| C[f,f] \right\rangle_\psi , \tag{G 17}$$

where we changed back to particle variables again and dropped the subscript f. With (G 17) instead of equation (48) in Catto *et al.* (2013), the additional squeezing factor that we get is retrieved and the result of (G 11) is corrected to agree with (G 5) .

G.2. *Small mean parallel velocity gradient*

We take the limit of small mean parallel velocity gradient and vanishing particle flux $\Gamma = 0$. In this limit we can compare our equations for particle flux (5.12) and energy flux (5.16) with those presented in Shaing & Hsu (2012).

We start by noting that the poloidal variation of the potential was neglected in Shaing & Hsu (2012). However, taking the limit of small mean parallel velocity gradient in (4.60) does not give $\phi_c = 0$ so the contribution from ϕ_θ should have been kept.

The first necessary step is to relate the functions G_1, G_2, H_1, H_2 with the functions μ_{1i}, μ_{2i} and μ_{3i} used in Shaing & Hsu (2012). Restricting our results to the case where $S > 0$, we find that

$$G_1 = 0.90\sqrt{\frac{R}{r}}\frac{S^{3/2}}{\nu}\mu_{1i}, \qquad H_1 = 0.68\sqrt{\frac{R}{r}}\frac{S^{3/2}}{\nu}\left[\mu_{2i} - \left(\bar{y}^2 - \frac{5}{2}\right)\mu_{1i}\right], \tag{G 18}$$

$$G_2 = -0.77\sqrt{\frac{R}{r}}\frac{S^{3/2}}{\nu}\mu_{2i}, \qquad H_2 = -2.74\sqrt{\frac{R}{r}}\frac{S^{3/2}}{\nu}\left[\mu_{3i} - \left(\bar{y}^2 - \frac{5}{2}\right)\mu_{2i}\right], \tag{G 19}$$

if we make the replacement

$$x\left(1 - 3\frac{\bar{y}^2}{x^2}\right)^2\left(1 + \frac{\bar{y}^2}{x^2}\right)^{-3/2} \longrightarrow \sqrt{|x^2 + \bar{z} - \bar{y}^2|} \tag{G 20}$$

in the definition of μ_{ji} for $j = 1, 2, 3$ in equation (52) in Shaing & Hsu (2012). Note, that we use x and $\bar{y}$ as defined in our calculation in section 5 and not as in Shaing & Hsu (2012). The discrepancy is caused by a combination of two effects. The poloidal variation of the electric field has been neglected reducing $\bar{z}$ to $\bar{z} = m\bar{u}^2/T$. Second, the trapped particle distribution function in (4.38) is different from the one in Shaing & Hsu (2012). Our expressions (4.39) and (4.38) almost match with the result in equation (40) in (Shaing *et al.* 1994*a*), which is

$$\frac{\partial g_0^t}{\partial w_f} = -\frac{I}{\Omega S}\frac{v^2 - 3(u + V_\parallel)^2}{v^2 + (u + V_\parallel)^2}\left(\frac{w_f}{w} - H\frac{w_f}{\langle w\rangle_\psi}\right)\mathcal{D}f_M(v_\parallel = -u), \tag{G 21}$$

where $H = 0$ for trapped particles and $H = 1$ for barely-passing particles. Equations (4.39) and (4.38) differ from (G 21) by a factor of $(v^2 - 3(u + V_\parallel)^2)/(v^2 + (u + V_\parallel)^2)$. This discrepancy was already pointed out in the Appendix of Catto *et al.* (2013). This discrepancy can be traced back to the moment approach used in Shaing & Hsu (2012) for which one assumes that

$$v_\parallel \hat{\boldsymbol{b}}\cdot\boldsymbol{\nabla}(v_\parallel B) - v_\parallel B^2\hat{\boldsymbol{b}}\cdot\boldsymbol{\nabla}\left(\frac{v_\parallel}{B}\right) = 2v_\parallel^2\hat{\boldsymbol{b}}\cdot\boldsymbol{\nabla}B \tag{G 22}$$

is small. However, this assumption only holds for $v_\parallel \sim \sqrt{\epsilon}v_t$, which is true only for weak radial electric fields in conventional neoclassical theory. In the case where the potential gradient is large such that $u \sim v_\parallel \sim v_t$, the trapped-barely-passing region is shifted to $w \sim \sqrt{\epsilon}v_t$ but $v_\parallel \sim v_t$ and (G 22) cannot be neglected.

Once we correct for this discrepancy and make the substitution (G 20), we can compare terms in the parallel viscous force $\langle \boldsymbol{B}\cdot\boldsymbol{\nabla}\cdot\boldsymbol{\pi}^{\rm SH}\rangle$ and heat viscous force $\langle \boldsymbol{B}\cdot\boldsymbol{\nabla}\cdot\boldsymbol{\Theta}^{\rm SH}\rangle$ in equation (45) and (46) of Shaing & Hsu (2012) with our forces $F_\parallel$ and Θ. We find

$$\langle \boldsymbol{B}\cdot\boldsymbol{\nabla}\cdot\boldsymbol{\pi}^{\rm SH}\rangle = BF_\parallel \tag{G 23}$$

and

$$\langle \boldsymbol{B}\cdot\boldsymbol{\nabla}\cdot\boldsymbol{\Theta}^{\rm SH}\rangle = -B\Theta + B\left(\frac{mV_\parallel(2u + V_\parallel)}{2T} - \frac{5}{2}\right)F_\parallel. \tag{G 24}$$

Shaing & Hsu (2012) state that $F_\parallel = 0$, so that these expressions reduce to

$$0 = \langle \boldsymbol{B}\cdot\boldsymbol{\nabla}\cdot\boldsymbol{\pi}^{\rm SH}\rangle \tag{G 25}$$

and the heat viscous force is related to the energy flux by

$$Q = -\frac{qTR}{m\Omega Br}\langle \boldsymbol{B}\cdot\boldsymbol{\nabla}\cdot\boldsymbol{\Theta}^{\rm SH}\rangle. \tag{G 26}$$

Note that setting $F_\parallel = 0$ is necessary to match the energy flux Q.

Explicitly, equation (5.4) for $\Gamma = 0$ and $\Omega/(Iv_t)(\partial V/\partial\psi) \ll 1$ reduces to

$$\left[\frac{\partial}{\partial\psi}\ln p + \frac{m\Omega(u + V_\parallel)}{IT}\right]G_1 = 1.17\frac{\partial T}{\partial\psi}G_2, \tag{G 27}$$

a_1	0.5951	b_1	1.0000	c_1	1.2648
a_2	0.3965	b_2	-0.0459	c_2	-0.2798
a_3	-1.2929	b_3	0.0038	c_3	1.3578
a_4	9.3942	b_4	-0.0007	c_4	9.0470
a_5	-0.0075			c_5	-0.0871

TABLE 1. Numerical values for the parameters of the functions in (H 1)-(H 3).

which can be rewritten using (G 18) and (G 19),

$$\frac{V_\parallel + u}{B} = -\frac{IcT}{Z^2 eB^2}\left(\frac{\partial}{\partial\psi}\ln p + \frac{\mu_{2i}}{\mu_{1i}}\frac{\partial}{\partial\psi}\ln T\right), \tag{G 28}$$

and is the same as equation (65) in Shaing & Hsu (2012). Similarly, the energy flux (5.8) simplifies to

$$Q = -1.71\sqrt{\frac{R}{r}}\frac{pq\nu I}{m\Omega^2 S^{3/2}}\Delta\bar{Q}\frac{\partial T}{\partial\psi}, \tag{G 29}$$

where we have substituted (G 27) into (5.8). We can now compare these expressions with corresponding equations (65) and (67) in Shaing & Hsu (2012). The energy flux (G 29) can be written as

$$Q = -pmq\frac{c^2 IR}{Z^2 e^2 B^2 r}\mu_{3i}\left(1 - \frac{\mu_{2i}^2}{\mu_{1i}\mu_{3i}}\right)\frac{\partial T}{\partial\psi}, \tag{G 30}$$

which is the same as equation (67) in Shaing & Hsu (2012). Hence, the particle flux equation and energy flux equation give the same result as the one in Shaing & Hsu (2012) in the limit $\Omega/(Iv_t)(\partial V/\partial\psi) \ll 1$ and $\Gamma = 0$ if the factors in μ_{ji} are corrected as indicated in (G 20).

Appendix H. Pedestal profiles

The realistic pedestal profiles of density, ion and electron temperature that we use to calculate example fluxes in section 6.3 are shown in figure 11. The profiles are based on those measured by Viezzer *et al.* (2016). The functions we use are

$$\bar{n} = a_1 + a_2\tanh[a_3(\bar{\psi} - a_4)] + a_5\bar{\psi}, \tag{H 1}$$

$$\bar{T} = b_1 + b_2\bar{\psi} + b_3\bar{\psi}^2 + b_3\bar{\psi}^3, \tag{H 2}$$

and

$$\bar{T}_e = c_1 + c_2\tanh[c_3(\bar{\psi} - c_4)] + c_5\bar{\psi}, \tag{H 3}$$

where the numerical parameters are given in table 1.

REFERENCES

CATTO, PETER J, BERNSTEIN, IRA B & TESSAROTTO, MASSIMO 1987 Ion transport in toroidally rotating tokamak plasmas. *The Physics of fluids* **30** (9), 2784–2795.

CATTO, PETER J, KAGAN, GRIGORY, LANDREMAN, MATT & PUSZTAI, ISTVAN 2011 A unified treatment of kinetic effects in a tokamak pedestal. *Plasma Physics and Controlled Fusion* **53** (5), 054004.

CATTO, PETER J, PARRA, FELIX I, KAGAN, GRIGORY, PARKER, JEFFREY B, PUSZTAI, ISTVAN & LANDREMAN, MATT 2013 Kinetic effects on a tokamak pedestal ion flow, ion heat transport and bootstrap current. *Plasma Physics and Controlled Fusion* **55** (4), 045009.

Churchill, RM, Theiler, C, Lipschultz, B, Hutchinson, IH, Reinke, ML, Whyte, D, Hughes, JW, Catto, P, Landreman, M, Ernst, D & others 2015 Poloidal asymmetries in edge transport barriers. *Physics of Plasmas* **22** (5), 056104.

Cruz-Zabala, DJ, Viezzer, E, Plank, U, McDermott, RM, Cavedon, M, Fable, E, Dux, R, Cano-Megias, P, Pütterich, T, van Vuuren, A Jansen & others 2022 In-out charge exchange measurements and 3d modelling of diagnostic thermal neutrals to study edge poloidal impurity asymmetries. *Plasma Physics and Controlled Fusion* **64** (4), 045021.

Greenfield, CM, Schissel, DP, Stallard, BW, Lazarus, EA, Navratil, GA, Burrell, KH, Casper, TA, DeBoo, JC, Doyle, EJ, Fonck, RJ & others 1997 Transport and performance in diii-d discharges with weak or negative central magnetic shear. *Physics of Plasmas* **4** (5), 1596–1604.

Hazeltine, RD 1989 Self-consistent radial sheath. *Physics of Fluids B: Plasma Physics* **1** (10), 2031–2039.

Hinton, FL & Hazeltine, Richard D 1976 Theory of plasma transport in toroidal confinement systems. *Reviews of Modern Physics* **48** (2), 239.

Hinton, FL & Wong, SK 1985 Neoclassical ion transport in rotating axisymmetric plasmas. *The Physics of fluids* **28** (10), 3082–3098.

Kagan, Grigory & Catto, Peter J 2008 Arbitrary poloidal gyroradius effects in tokamak pedestals and transport barriers. *Plasma Physics and Controlled Fusion* **50** (8), 085010.

Kagan, Grigory & Catto, Peter J 2010 Neoclassical ion heat flux and poloidal flow in a tokamak pedestal. *Plasma Physics and Controlled Fusion* **52** (5), 055004.

Landreman, Matt, Parra, Felix I, Catto, Peter J, Ernst, Darin R & Pusztai, Istvan 2014 Radially global δf computation of neoclassical phenomena in a tokamak pedestal. *Plasma Physics and Controlled Fusion* **56** (4), 045005.

McDermott, RM, Lipschultz, B, Hughes, JW, Catto, PJ, Hubbard, AE, Hutchinson, IH, Granetz, RS, Greenwald, M, LaBombard, B, Marr, K & others 2009 Edge radial electric field structure and its connections to h-mode confinement in alcator c-mod plasmas. *Physics of Plasmas* **16** (5), 056103.

Parra, Felix I & Catto, Peter J 2008 Limitations of gyrokinetics on transport time scales. *Plasma Physics and Controlled Fusion* **50** (6), 065014.

Shaing, KC & Hsu, CT 2012 Neoclassical theory inside transport barriers in tokamaks. *Physics of Plasmas* **19** (2), 022502.

Shaing, Ker-Chung & Hazeltine, RD 1992 Effects of orbit squeezing on ion transport in the banana regime in tokamaks. *Physics of Fluids B: Plasma Physics* **4** (8), 2547–2551.

Shaing, Ker-Chung, Hsu, CT & Dominguez, N 1994*a* Resonance parallel viscosity in the banana regime in poloidally rotating tokamak plasmas. *Physics of plasmas* **1** (5), 1168–1176.

Shaing, Ker-Chung, Hsu, CT & Hazeltine, RD 1994*b* Effects of orbit squeezing on poloidal mass flow and bootstrap current in tokamak plasmas. *Physics of plasmas* **1** (10), 3365–3368.

Theiler, C, Churchill, RM, Lipschultz, B, Landreman, M, Ernst, DR, Hughes, JW, Catto, PJ, Parra, FI, Hutchinson, IH, Reinke, ML & others 2014 Inboard and outboard radial electric field wells in the h-and i-mode pedestal of alcator c-mod and poloidal variations of impurity temperature. *Nuclear Fusion* **54** (8), 083017.

Viezzer, Eleonora, Cavedon, M, Cano-Megias, Pilar, Fable, E, Wolfrum, Elisabeth, Cruz-Zabala, Diego José, David, P, Dux, R, Fischer, R, Harrer, GF & others 2020 Dynamics of the pedestal transport during edge localized mode cycles at asdex upgrade. *Plasma Physics and Controlled Fusion* **62** (2), 024009.

Viezzer, Eleonora, Cavedon, Marco, Fable, Emiliano, Laggner, Florian M, McDermott, Rachael M, Galdon-Quiroga, Joaquin, Dunne, Mike G, Kappatou, Athina, Angioni, Clemente, Cano-Megias, P & others 2018 Ion heat transport dynamics during edge localized mode cycles at asdex upgrade. *Nuclear Fusion* **58** (2), 026031.

Viezzer, Eleonora, Fable, E, Cavedon, M, Angioni, C, Dux, R, Laggner, FM, Bernert, M, Burckhart, A, McDermott, RM, Pütterich, T & others 2016 Investigation of inter-elm ion heat transport in the h-mode pedestal of asdex upgrade plasmas. *Nuclear Fusion* **57** (2), 022020.

Viezzer, E, Pütterich, T, Conway, GD, Dux, R, Happel, T, Fuchs, JC, McDermott, RM, Ryter, F, Sieglin, B, Suttrop, W & others 2013 High-accuracy characterization of the edge radial electric field at asdex upgrade. *Nuclear Fusion* **53** (5), 053005.

Wagner, Fritz, Fussmann, G, Grave, T, Keilhacker, M, Kornherr, M, Lackner, K, McCormick, K, Müller, ER, Stäbler, A, Becker, G & others 1984 Development of an edge transport barrier at the h-mode transition of asdex. *Physical Review Letters* **53** (15), 1453.

Walk, JR, Hughes, JW, Hubbard, AE, Terry, JL, Whyte, DG, White, AE, Baek, SG, Reinke, ML, Theiler, C, Churchill, RM & others 2014 Edge-localized mode avoidance and pedestal structure in i-mode plasmas. *Physics of Plasmas* **21** (5), 056103.

Ware, AA 1970 Pinch effect for trapped particles in a tokamak. *Physical Review Letters* **25** (1), 15.